FINAL REPORT

Grant Title and Number:

Development of Fast Integral Solver in Time and Frequency Domains

F49620-01-1-0504

Period of Performance: **September 01, 01 – May 31, 05**

Principal Investigator: **Elizabeth H. Bleszynski**

MONOPOLE RESEARCH
739 Calle Sequoia, Thousand Oaks, CA 91360
tel: (805) 375-0318 fax: (805) 499-9878

Approved for public release, distribution unlimited

REPORT DOCUMENTATION PAGE

AFRL-SR-AR-TR-05-
0468

1. AGENCY USE ONLY (Leave Blank)	2. REPORT DATE	3. REPORT TYPE AND DATES COVERED
	25 October, 2005	01 October, 03 – 31 May 05

4. TITLE AND SUBTITLE
Development of fast integral solver in time and frequency domains

5. FUNDING NUMBERS
Grant F49620-01-1-0504

6. AUTHOR(S)
Elizabeth Bleszynski, Marek Bleszynski, Thomas Jaroszewicz

7. PERFORMING ORGANIZATION NAME(S) AND ADDRESS(ES)
Monopole Research
739 Calle Sequoia, Thousand Oaks, CA 91360

8. PERFORMING ORGANIZATION REPORT NUMBER
MON- -2005-10

9. SPONSORING / MONITORING AGENCY NAME(S) AND ADDRESS(ES)
Air Force Office of Scientific Research
875 North Randolph Rd., Ste 325, Room 3112
Arlington, VA 22203

10. SPONSORING / MONITORING AGENCY REPORT NUMBER

11. SUPPLEMENTARY NOTES
The views, opinions and/or findings contained in this report are those of the author(s) and should not be construed as an official Department of the Air Force position, policy or decision, unless so designated by other documentation.

12 a. DISTRIBUTION / AVAILABILITY STATEMENT
Approved for public release, distribution unlimited. NM

12 b. DISTRIBUTION CODE

13. ABSTRACT (Maximum 200 words)

We constructed a new time domain algorithm which is particularly well suited to general dispersive media with penetrable and impenetrable surface and bulk volumetric properties. The algorithm complexity does not depend on the degree of dispersion. The algorithm small computational cost (O(Nt Ns logNt logNs) and O(Nt Ns**4/3 logNt logNs) for volume and surface problems respectively, where Nt and Ns denote the number of temporal and spatial samples) is achieved through the simultaneous application of Fast Fourier Transforms in space and time. The algorithm is based on a new formulation of integral equations: instead of using the customary integral equations involving the Green function and its derivatives, we constructed supplemental integral equation operators equal to the Fourier transform of the dispersive medium Green function, to the Fourier transform of the product of the dispersive medium Green function with the frequency dependent dielectric permittivity, and to the Fourier transform of the product of the dispersive medium Green function with the inverse of the dielectric permittivity. The algorithm does not require analytical representation of the (dispersive) medium Green function and, in particular, it can be used with a medium Green function given in a tabular form. The algorithm is already being successfully used for the simulation of SAR imaging and in the context of electronic packaging.

14. SUBJECT TERMS
time domain integral equations, foliage penetration, computational electromagnetics, dispersive media, conducting Debye medium,

15. NUMBER OF PAGES
21

16. PRICE CODE

17. SECURITY CLASSIFICATION OR REPORT	18. SECURITY CLASSIFICATION ON THIS PAGE	19. SECURITY CLASSIFICATION OF ABSTRACT	20. LIMITATION OF ABSTRACT
UNCLASSIFIED	UNCLASSIFIED	UNCLASSIFIED	UL

TABLE OF CONTENTS

1. Objectives

The main focus of the work was the ***development of a fast time-domain algorithm for solving Maxwell's equations in the integral form for general dispersive media with both penetrable and impenetrable surface and bulk volumetric properties.*** The main motivation for this work was the need for an integral equation solver applicable to the description of propagation of wide-band pulses through different types of dispersive media including those which are of interest in the context of foliage penetration.

During the course of the project we have been working closely on related applications of the fast integral equation solver with the Brooks Air Force Base Mathematical Products Group lead by Dr. R. Albanese.

2. Main accomplishments

We summarize the main developments carried out on this project.

We constructed a new time-domain algorithm which is particularly well suited to general dispersive media with both penetrable and impenetrable surface and bulk volumetric properties. The algorithm is described in [5] and in the first yearly report. The main features of the algorithm are as follows:

(i) The algorithm complexity does not depend on the degree of dispersion. Its small computational cost ($O(N_t\, N_s \log N_t \log N_s)$ and $O(N_t\, N_s^{4/3} \log N_t \log N_s)$ for volume and surface problems respectively, where N_t and N_s denote the number of temporal and spatial samples) is achieved through the ***simultaneous application of Fast Fourier Transforms in space and time***. We stress that algorithm is applicable to both

(i1) conventional volumetric integral (involving free space Green's function and volumetric discretization) equations for dispersive media

and to

(i2) (much more difficult in terms of formulation, analytical and numerical implementation, but significantly more beneficial in terms of algorithm complexity) equivalent current surface integral equations for a general piecewise homogeneous dispersive dielectric medium with dispersive thin sheet material interfaces. (We note that the main part of our effort was devoted to such integral equations.)

(ii) The algorithm is based on a new ***formulation of integral equations specially tailored to problems involving dispersive media.*** The formulation is both general and significantly simpler than the conventional approaches: instead of using the customary integral equation operators involving the Green function and its derivatives, we construct **supplemental integral equation operators** equal (a) to the Fourier transform of the dispersive medium Green function, (b) to the Fourier transform of the product of the dispersive medium Green function with the frequency dependent dielectric permittivity, and, (c) to the Fourier transform of the product of the dispersive medium Green function with the inverse of the dielectric permittivity. An important benefit of such an approach is that the resulting integrals involve only single (and not

double) time convolutions. The formulation is applicable to systems involving bulk dispersive regions and thin dispersive sheets represented as interfaces. We have carried out complete analytical calculations and corresponding numerical procedures for the evaluation of matrix elements of the integral operators, executed in the framework of the full Galerkin scheme in space and time variables, for the "conductive Debye medium" (i.e., for a medium with the electric permittivity given by the Debye formula supplemented with a term responsible for the medium conductivity). The procedure employs a suitable contour integration around singularities of the effective Green function operators in the complex frequency plane.

(iii) ***The algorithm does not require analytical representation of the (dispersive) medium Green function and, in particular, can be used with a medium Green function given in a tabular form.***

(iv) Our formulation provides a framework and a practical tool for an accurate numerical simulation framework for a variety of problems involving wide band pulse propagation, including wide band antenna pattern simulation or propagation of narrow pulses through dispersive media. Such applications require the numerical capability of propagating an ultrawideband pulse in a dispersive environment over several absorption lengths. In particular, such numerical capability appears to be necessary in studies of an intriguing phenomenon of a Brillouin precursor, a propagating structure which, because of its non-exponential peak decay, may lead to multiple potential applications, including detection of objects in cluttered environments.

We note that our work on this project had a ***significant impact on the CEM academic and industrial community.*** In particular an early version of the block Toeplitz time-domain integral equation solver we proposed has been independently verified and adopted as the Time Domain Adaptive Integral Equation Method by the University of Illinois researches who constructed a code based on this formulation [3]. Also researches in Motorola and Cadence [4] apply the method in the context of electronic packaging.

3. Technical details

In this Section we describe in more detail the relevant aspects associated with the formulation and implementation of the approach.

(A.) Time-domain electric-field integral equations for dispersive media

The integral equation formulation we developed is ***particularly suitable to problems involving dispersive media***. We constructed a ***general set of integral equations, significantly simpler than the conventional formulation***; instead of using the customary integral equation operators equal to the Green functions $\widetilde{g}(\omega,\mathbf{r})$ and their derivatives, we use ***supplemental integral equation operators*** $K_0(t,\mathbf{r})$, $K_1(t,\mathbf{r})$, and $K_2(t,\mathbf{r})$ equal to the Fourier transforms of the Green function of the dispersive medium and their products with frequency dependent dielectric permittivity

$$g(t,\mathbf{r}) = \int \frac{\mathrm{d}\omega}{2\pi}\, \mathrm{e}^{-\mathrm{i}\omega t}\, \widetilde{g}(\omega,\mathbf{r})\ , \tag{3.1a}$$

$$g_1(t,\mathbf{r}) = \int \frac{\mathrm{d}\omega}{2\pi}\, \frac{1}{\widetilde{\epsilon}(\omega)}\, \mathrm{e}^{-\mathrm{i}\omega t}\, \widetilde{g}(\omega,\mathbf{r})\ , \tag{3.1b}$$

$$g_2(t,\mathbf{r}) = \int \frac{\mathrm{d}\omega}{2\pi}\, \widetilde{\epsilon}(\omega)\, \mathrm{e}^{-\mathrm{i}\omega t}\, \widetilde{g}(\omega,\mathbf{r})\ . \tag{3.1c}$$

An important benefit of such formulation is its generality, simplicity and efficiency. The resulting integrals involve only ***single*** (not double) time convolutions, i.e., the resulting integral equations have the schematic structure $\int K(t-t')\,X(t')\,\mathrm{d}t' = B(t)$, instead of $\int K_1(t-t'')\,K_2(t''-t')\,X(t')\,\mathrm{d}t''\,\mathrm{d}t' = B(t)$.

In terms of $g(t,\mathbf{r})$, $g_1(t,\mathbf{r})$, and $g_2(t,\mathbf{r})$ the surface integral equations for a general piecewise homogeneous dispersive dielectric medium with dispersive thin sheet material interfaces take the form

$$\frac{1}{c}\int \mathrm{d}t' \begin{bmatrix} R(t-t',\mathbf{r}) & U(t-t',\mathbf{r})\,\mathbf{n}(\mathbf{r})\times \\ U(t-t',\mathbf{r})\,\mathbf{n}(\mathbf{r})\times & S(t-t',\mathbf{r}) \end{bmatrix} \begin{bmatrix} \mathbf{J}(t',\mathbf{r}) \\ \mathbf{M}(t',\mathbf{r}) \end{bmatrix}$$
$$+\int \mathrm{d}t' \int\limits_{\Sigma} d^2S' \begin{bmatrix} K_{11}(t-t',\mathbf{r}-\mathbf{r}') & K_{12}(t-t',\mathbf{r}-\mathbf{r}') \\ K_{21}(t-t',\mathbf{r}-\mathbf{r}') & K_{22}(t-t',\mathbf{r}-\mathbf{r}') \end{bmatrix} \begin{bmatrix} \mathbf{J}(t',\mathbf{r}') \\ \mathbf{M}(t',\mathbf{r}') \end{bmatrix} = \begin{bmatrix} \mathbf{E}^{\mathrm{i}}(t,\mathbf{r}) \\ \mathbf{H}^{\mathrm{i}}(t,\mathbf{r}) \end{bmatrix} \tag{3.2}$$

with the kernels K_{ij} given by

$$K_{11}(t-t',\mathbf{r}-\mathbf{r}') = \frac{\widetilde{\mu}}{c^2}\,\partial_t\, g(t-t',\mathbf{r}-\mathbf{r}') - \nabla\nabla\cdot \int\limits_{-\infty}^{t} \mathrm{d}\tau\, g_1(\tau-t',\mathbf{r}-\mathbf{r}')\ ,$$

$$K_{12}(t-t',\mathbf{r}-\mathbf{r}') = \quad c^{-1}\,\nabla\times g(t-t',\mathbf{r}-\mathbf{r}')\ ,$$

$$K_{21}(t-t',\mathbf{r}-\mathbf{r}') = -c^{-1}\,\nabla\times g(t-t',\mathbf{r}-\mathbf{r}')\ ,$$

$$K_{22}(t-t',\mathbf{r}-\mathbf{r}') = \frac{1}{c^2}\,\partial_t\, g_2(t-t',\mathbf{r}-\mathbf{r}') - \frac{1}{\widetilde{\mu}}\nabla\nabla\cdot \int\limits_{-\infty}^{t} \mathrm{d}\tau\ g(\tau-t',\mathbf{r}-\mathbf{r}')\ , \tag{3.3}$$

In the above equation $\widetilde{R}(t,\mathbf{r})$, $\widetilde{S}(t,\mathbf{r})$, and $\widetilde{U}(t,\mathbf{r})$ represent the Fourier transforms of the respective functions $\widetilde{R}(\omega,\mathbf{r})$, $\widetilde{S}(\omega,\mathbf{r})$, and $\widetilde{U}(\omega,\mathbf{r})$ representing the dimensionless electric, magnetic, and "cross-" resistivities of the mathematically infinitely thin sheet material interfaces [1] between two homogeneous volumetric regions, and $\mathbf{J}(t,\mathbf{r})$ and $\mathbf{M}(t,\mathbf{r})$ are the unknown vector functions: equivalent electric and magnetic currents on material interfaces.

We note that in (3.3) we assumed, for simplicity, that $\widetilde{\mu}(\omega) = \text{const}$. Generalization to dispersive $\widetilde{\mu}(\omega)$ is straightforward.

An alternative set of equations, obtained by taking the negative time derivative of (3.2) is

$$\frac{1}{c}\int \mathrm{d}t' \begin{bmatrix} \partial_t R(t-t',\mathbf{r}) & \partial_t U(t-t',\mathbf{r})\,\mathbf{n}(\mathbf{r})\times \\ \partial_t U(t-t',\mathbf{r})\,\mathbf{n}(\mathbf{r})\times & \partial_t S(t-t',\mathbf{r}) \end{bmatrix} \begin{bmatrix} \mathbf{J}(t',\mathbf{r}) \\ \mathbf{M}(t',\mathbf{r}) \end{bmatrix}$$
$$+ \int \mathrm{d}t' \int\limits_{\Sigma} d^2S' \begin{bmatrix} K_{11}(t-t',\mathbf{r}-\mathbf{r}') & K_{12}(t-t',\mathbf{r}-\mathbf{r}') \\ K_{21}(t-t',\mathbf{r}-\mathbf{r}') & K_{22}(t-t',\mathbf{r}-\mathbf{r}') \end{bmatrix} \begin{bmatrix} \mathbf{J}(t',\mathbf{r}') \\ \mathbf{M}(t',\mathbf{r}') \end{bmatrix} = \partial_t \begin{bmatrix} \mathbf{E}^{\mathrm{i}}(t,\mathbf{r}) \\ \mathbf{H}^{\mathrm{i}}(t,\mathbf{r}) \end{bmatrix}, \quad (3.4)$$

with

$$\begin{aligned} K_{11}(t-t',\mathbf{r}-\mathbf{r}') &= \frac{\widetilde{\mu}}{c^2}\,\partial_t^2\, g(t-t',\mathbf{r}-\mathbf{r}') - \nabla\nabla\cdot\, g_1(t-t',\mathbf{r}-\mathbf{r}')\,, \\ K_{12}(t-t',\mathbf{r}-\mathbf{r}') &= \quad c^{-1}\,\nabla\times\,\partial_t\, g(t-t',\mathbf{r}-\mathbf{r}')\,, \\ K_{21}(t-t',\mathbf{r}-\mathbf{r}') &= -c^{-1}\,\nabla\times\,\partial_t\, g(t-t',\mathbf{r}-\mathbf{r}')\,, \\ K_{22}(t-t',\mathbf{r}-\mathbf{r}') &= \frac{1}{c^2}\,\partial_t^2\, g_2(t-t',\mathbf{r}-\mathbf{r}') - \frac{1}{\widetilde{\mu}}\nabla\nabla\cdot\, g(t-t',\mathbf{r}-\mathbf{r}')\,. \end{aligned} \quad (3.5)$$

We stress that both the fast FFT solution scheme [5] and the complete Galerkin discretization method in space and time which we discuss below, are applicable to Eqs. (3.2) as well as (3.4).

(B.) Complete Galerkin discretization procedure in spatial and temporal variables

We developed an ***accurate method of the treatment of the causal behavior of the time-domain Green function*** achieved through the utilization of the ***complete Galerkin procedure in spatial and temporal variables*** in the evaluation of impedance matrix elements.

It has been known, in general, that the use of the Galerkin method constitutes a key element in achieving numerical stability of the solution schemes for time-domain integral equation approaches. Although for one-dimensional wave propagation problems implementation of the causality of the Green function in the context of the Galerkin discretization is relatively straightforward, implementation of the causality in three dimensions presents a much more complicated task for the following two reasons:

(a.) The Green function depends on the relative time τ and distance $r = |\mathbf{r}_1 - \mathbf{r}_2|$. If the basis functions have a certain spatial extent, the signal from one basis function may, in general, arrive only to a portion of the other basis function. Implementation of causality requires careful implementation of all relevant radial integrals over the spatial coordinates $\mathbf{r}_1$ and $\mathbf{r}_2$ associated with the basis functions entering the matrix element.

(b.) The three-dimensional Green function has a singular term associated with $1/r = 1/|\mathbf{r}_1 - \mathbf{r}_2|$, which is in practice rather difficult to take into account in the context of three-dimensional integrals over vector variables $\mathbf{r}_1$ and $\mathbf{r}_2$.

We implemented routines for an efficient and accurate evaluation of the spatial separation densities $\langle \hat{\rho}_{\alpha\beta}(r) \rangle$ (defined as angular averages of convolutions of pairs of spatial basis functions) for Rao-Glisson-Wilton basis functions. In Figs. 1a through 1f below we display some numerical results for the separation densities calculated according to our prescription, associated with various components of the Green function. Numerical values of the separation densities obtained using our approach compare almost exactly with the analytically equivalent but numerically much more intensive expressions involving direct 3-dimensional numerical integration quadratures.

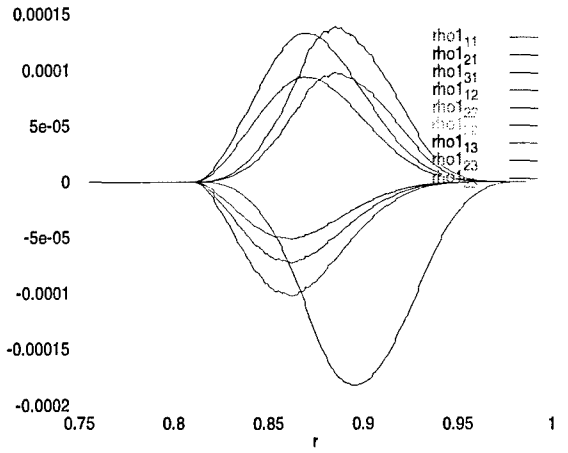

Fig. 1a: Numerical values of separation densities associated with 9 components of the tensor Green function for the configuration of 2 triangles in the far-field zone.

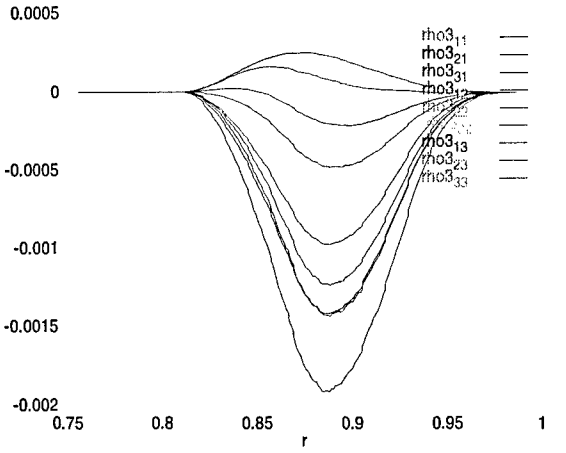

Fig. 1b: Numerical values of separation densities associated with 9 components of the vector Green function for the configuration of 2 triangles in the far-field zone.

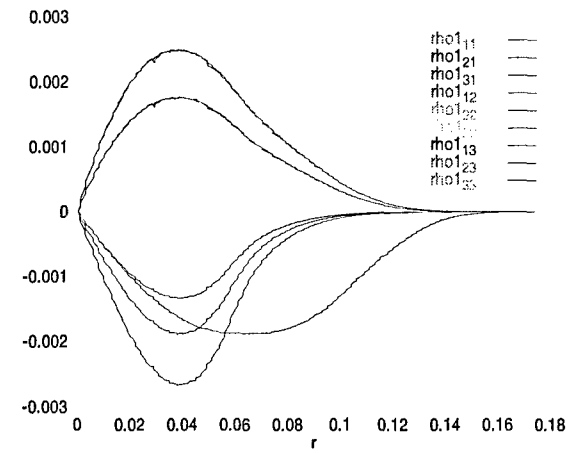

Fig. 1c: Numerical values of separation densities associated with 9 components of the tensor Green function for configuration of 2 adjacent triangles (near field zone).

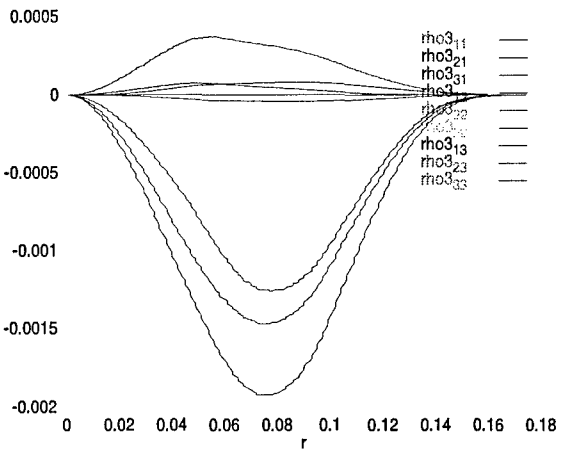

Fig. 1d: Numerical values of separation densities associated with 9 components of the vector Green function for the configuration of 2 adjacent triangles (near-field zone).

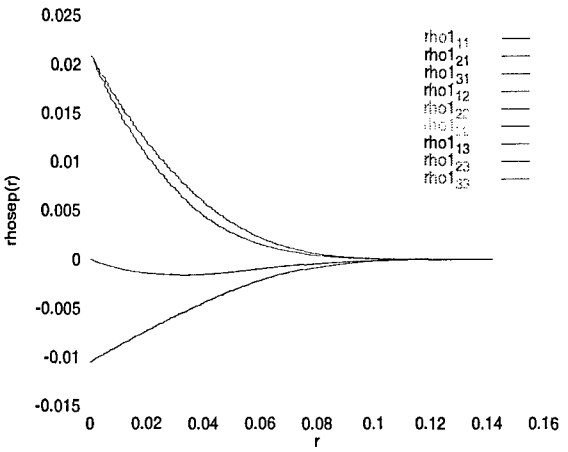

Fig. 1e: Numerical values of separation densities associated with 9 components of the tensor Green function for the configuration of 2 overlapping triangles (self-field zone).

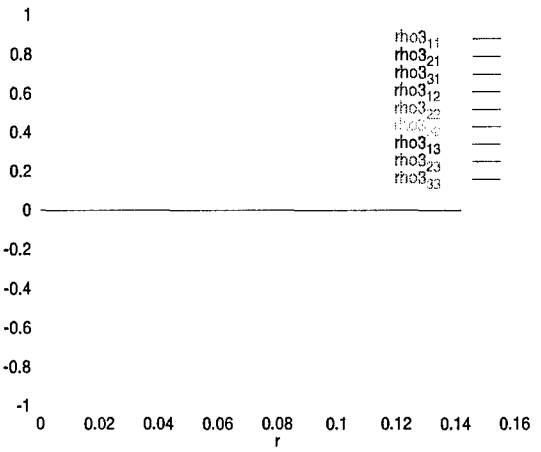

Fig. 1f: Numerical values of separation densities associated with 9 components of the vector Green function for the configuration of 2 overlapping triangles (self-field zone).

More details on this part of the project were reported in the second yearly progress report and published in [5].

(C.) Formulation for a conductive Debye medium

We have carried out complete analytical calculations for a specific, and general model of a "conductive Debye medium", with the electric permittivity given by the Debye formula supplemented with a term responsible for conductivity,

$$\widetilde{\epsilon}(\omega) = \epsilon_\infty + \frac{\epsilon_s - \epsilon_\infty}{1 - i\tau\omega} + i\frac{\nu}{\omega} \,. \tag{3.6}$$

In Eq.(3.6) ϵ_s and ϵ_∞ are the static and optical relative permittivities, τ is the relaxation time, and $\nu = \sigma/\epsilon_0 = c\,Z_0\,\sigma$ is a parameter proportional to the conductivity σ, having the dimension of frequency. Analyticity requires real ϵ_s and ϵ_∞, and we assume, additionally, that $\epsilon_s \geq \epsilon_\infty$.

The parameterization (3.6) reduces to the following cases:

$$\widetilde{\epsilon}(\omega) = \begin{cases} \epsilon_\infty & \text{(non-dispersive medium)} \quad \text{for } \nu = 0,\ \tau = \infty \,, \\ \epsilon_\infty + \dfrac{\epsilon_s - \epsilon_\infty}{1 - i\tau\omega} & \text{(Debye medium)} \quad \text{for } \nu = 0 \,, \\ \epsilon_\infty + i\dfrac{\nu}{\omega} & \text{(lossy medium)} \quad \text{for } \tau = \infty \,. \end{cases} \tag{3.7}$$

To exhibit the analytic structure of the electric permittivity function we now rewrite Eq.(3.6) as

$$\widetilde{\epsilon}(\omega) = \epsilon_\infty \frac{(\omega - \omega_1)\,(\omega - \omega_2)}{\omega\,(\omega - \omega_3)} \,, \tag{3.8}$$

where

$$\omega_1 = \frac{i}{2\,\epsilon_\infty\,\tau}\left[-(\epsilon_s + \nu\tau) + \sqrt{(\epsilon_s - \nu\tau)^2 + 4\,(\epsilon_s - \epsilon_\infty)\,\nu\tau}\right] \,, \tag{3.9a}$$

$$\omega_2 = \frac{i}{2\,\epsilon_\infty\,\tau}\left[-(\epsilon_s + \nu\tau) - \sqrt{(\epsilon_s - \nu\tau)^2 + 4\,(\epsilon_s - \epsilon_\infty)\,\nu\tau}\right] \,, \tag{3.9b}$$

$$\omega_3 = -\frac{i}{\tau} \,. \tag{3.9c}$$

Thus, as required by the analyticity (causality) properties, $\widetilde{\epsilon}(\omega)$ is analytic in the upper half-plane of ω; it has two poles (at zero and on the negative imaginary axis, at ω_3), as well as two zeros, also located on the negative imaginary axis.

The wave number is then

$$k(\omega) = \frac{\omega}{c}\sqrt{\widetilde{\epsilon}(\omega)\,\widetilde{\mu}(\omega)} = \frac{1}{v}\sqrt{\frac{\omega\,(\omega - \omega_1)\,(\omega - \omega_2)}{\omega - \omega_3}} \,, \tag{3.10}$$

where $c = 1/\sqrt{\epsilon_0\,\mu_0}$ and

$$v = \frac{c}{\sqrt{\epsilon_\infty}} \,. \tag{3.11}$$

The expression (3.10) has thus branch points at $\omega = 0$ and $\omega = \omega_n$, $n = 1, 2, 3$.

Since, for typical parameters, we have

$$0 \leq |\omega_1| \leq |\omega_3| \leq |\omega_2| \,, \tag{3.12}$$

it is convenient to define branch cuts in the ω plane as in Fig. 2.

We have constructed both analytical representations and numerical procedures for computing matrix elements of the integral operators for the above mentioned medium, employing full Galerkin procedure in space and time.

The analytical calculations are reported in Appendix A1 of the second yearly report. The final result is a set of expressions for matrix elements of the Green functions g, g_1, and g_2 of Eq.(3.1) which can be represented, schematically, as

$$\begin{aligned} A^{\mu}_{\alpha\beta} &\equiv \int \mathrm{d}t_1 \, \mathrm{d}^2 r_1 \, \mathrm{d}2_1 \, \mathrm{d}^2 r_2 \, T^{\mu}(t_1) \, \mathbf{\Psi}_{\alpha}(\mathbf{r}_1) \cdot g(t_1 - t_2, \mathbf{r}_1 - \mathbf{r}_2) \, T^{0}(t_2) \, \mathbf{\Psi}_{\beta}(\mathbf{r}_2) \\ &= \int_0^{\infty} \mathrm{d}r \, \langle \hat{\rho}_{\alpha\beta}(r) \rangle \, f^{\mu}(r) \,. \end{aligned} \tag{3.13}$$

Here $A^{\mu}_{\alpha\beta}$ is the matrix element computed between temporal basis functions T of time separation $\mu \, \Delta t$ (where Δt is the time step), and spatial basis functions $\mathbf{\Psi}$ associated with current elements (edges of the discretization) α and β. The actual matrix elements may also involve Green functions g_1 and g_2, or their time derivatives or integrals, and spatial differential operators (divergence and curl) acting either on the Green functions or on the spatial basis functions.

Eq.(3.13) represents the matrix element as a space integral of the ***"spatial separation density"*** $\langle \hat{\rho}_{\alpha\beta}(r) \rangle$ (expressible in terms of the basis functions $\mathbf{\Psi}_{\alpha}$ and $\mathbf{\Psi}_{\beta}$) and functions f^{μ} constructed from the Green function and the spatial basis functions. All the dependence on the medium properties and its dispersion is thus contained in the functions f^{μ}.

In Appendix A1 of the second yearly report we described in detail evaluation of the spatial separation densities $\langle \hat{\rho} \rangle$ and provide semi-analytic expression for their efficient computation. We also give a details of the procedure for computing the functions f^{μ}: in the general case of the conductive Debye medium (Eq.(3.6)) they are given as frequency integrals over the frequency-domain Green functions and Fourier transforms of ***"temporal separation densities"*** $\eta^{\mu}(t)$, defined in analogy to $\langle \hat{\rho}_{\alpha\beta} \rangle$ as convolutions of temporal basis functions. The frequency integrals are evaluated by deforming the integration contour to one encircling singularities of $\widetilde{\epsilon}(\omega)$ and $\sqrt{\widetilde{\epsilon}(\omega)}$, which are located on the imaginary ω axis; hence the expressions involve also Laplace transforms of the temporal separation densities $\eta^{\mu}(t)$, which can be evaluated analytically. The resulting frequency integrals can be efficiently and accurately computed as numerical quadratures. Some of these integrals, however, have to be treated with special care: this applies to cases when a pole in the integrand coincides with a branch point (which is also an essential singularity).

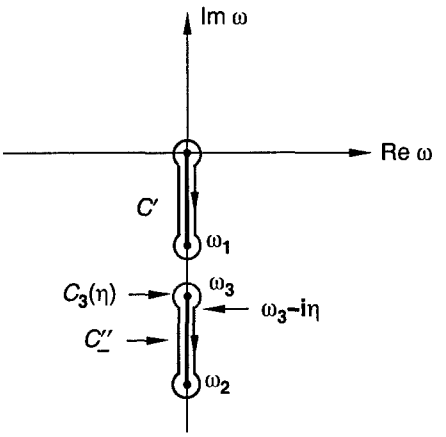

Fig. 2: The singularity structure of the electric permittivity function and the integration used in evaluation of the Green function.

We present here more details of the computation of the time-domain Green functions $g(t,\mathbf{r})$, $g_1(t,\mathbf{r})$ and $g_2(t,\mathbf{r})$ of Eqs. (3.1) in the case of the conductive Debye medium (Eq.(3.6)). First we consider the function $g(t,\mathbf{r})$ of Eq.(3.1a) defined as

$$g(t,r) = \int \frac{\mathrm{d}\omega}{2\pi}\, \mathrm{e}^{-\mathrm{i}\omega t}\, \widetilde{g}(\omega,r) = \frac{1}{4\pi r} \int \frac{\mathrm{d}\omega}{2\pi}\, \mathrm{e}^{-\mathrm{i}\omega t}\, \mathrm{e}^{\mathrm{i}\, k(\omega)\, r} \ . \tag{3.14}$$

It is convenient to start with evaluating the corresponding Green function in one spatial dimension, where, in frequency domain

$$\hat{\widetilde{g}}(\omega,r) = \frac{\mathrm{i}}{2\, k(\omega)}\, \mathrm{e}^{\mathrm{i}\, k(\omega)\, r} \ , \tag{3.15}$$

and thus the corresponding Green function in three dimensions is

$$\widetilde{g}(\omega,r) = \frac{1}{4\pi\, r}\, \mathrm{e}^{\mathrm{i}\, k(\omega)\, r} = -\frac{1}{2\pi\, r}\, \frac{\partial}{\partial r}\, \hat{g}(\omega,r) \ . \tag{3.16}$$

Now, for the one-dimensional case, the integral

$$\begin{aligned} \hat{g}(t,r) &= \int \frac{\mathrm{d}\omega}{2\pi}\, \frac{\mathrm{i}}{2\, k(\omega)}\, \mathrm{e}^{-\mathrm{i}\omega t}\, \mathrm{e}^{\mathrm{i}\, k(\omega)\, r} \\ &= \frac{\mathrm{i}v}{2} \int \frac{\mathrm{d}\omega}{2\pi} \sqrt{\frac{\omega-\omega_3}{\omega\,(\omega-\omega_1)\,(\omega-\omega_2)}}\, \mathrm{e}^{-\mathrm{i}\omega t}\, \exp\left(\mathrm{i}\sqrt{\frac{\omega\,(\omega-\omega_1)\,(\omega-\omega_2)}{\omega-\omega_3}}\, \frac{r}{v}\right) \end{aligned} \tag{3.17}$$

is convergent, and can be evaluated by deforming the original integration contour along the real axis on the ω-plane into the contours C' and C'' of Fig. 2. In the latter contours we include circles around singular points; in some cases these circles give nonzero contributions.

By analyzing the phase changes on encircling the branch points, we find that the square root appearing in the exponential of Eq.(3.17) is real positive just to the right of the branch cuts, and real negative just to the left of these cuts. Then, by changing the integration variable to $u = \mathrm{i}\omega$, and denoting $\omega_n = -\mathrm{i}u_n$ with $\mathrm{Re}\, u_n \geq 0$, $n = 1, 2, 3$, we obtain

$$\hat{g}(t,r) = \frac{v}{2}\,\Theta\left(t - \frac{r}{v}\right)\left\{\int_0^{u_1}\frac{\mathrm{d}u}{2\pi}\,\frac{1}{f(u)}\,\mathrm{e}^{-ut}\,\mathrm{e}^{\mathrm{i}\,f(u)\,r/v} + \int_{u_3}^{u_2}\frac{\mathrm{d}u}{2\pi}\,\frac{1}{f(u)}\,\mathrm{e}^{-ut}\,\mathrm{e}^{\mathrm{i}\,f(u)\,r/v}\right.$$

$$\left. - \int_0^{u_1}\frac{\mathrm{d}u}{2\pi}\,\frac{-1}{f(u)}\,\mathrm{e}^{-ut}\,\mathrm{e}^{-\mathrm{i}\,f(u)\,r/v} - \int_{u_3}^{u_2}\frac{\mathrm{d}u}{2\pi}\,\frac{-1}{f(u)}\,\mathrm{e}^{-ut}\,\mathrm{e}^{-\mathrm{i}\,f(u)\,r/v}\right\}$$

$$= v\,\Theta\left(t - \frac{r}{v}\right)\left\{\int_0^{u_1}\frac{\mathrm{d}u}{2\pi}\,\frac{1}{f(u)}\,\mathrm{e}^{-ut}\,\cos\left(f(u)\,\frac{r}{v}\right) + \int_{u_3}^{u_2}\frac{\mathrm{d}u}{2\pi}\,\frac{1}{f(u)}\,\mathrm{e}^{-ut}\,\cos\left(f(u)\,\frac{r}{v}\right)\right\}, \quad (3.18)$$

where Θ is the Heaviside step function and

$$f(u) = \sqrt{-\frac{u\,(u-u_1)\,(u-u_2)}{u-u_3}} \quad (3.19)$$

is defined to be positive in the u intervals occurring in Eq.(3.18).

According to Eq.(3.16), the corresponding Green function in three dimensions is then

$$g(t,r) \equiv g(t,\mathbf{r}) = \frac{1}{2\pi r}\,\delta\left(t - \frac{r}{v}\right)\left\{\int_0^{u_1} + \int_{u_3}^{u_2}\right\}\frac{\mathrm{d}u}{2\pi}\,\frac{1}{f(u)}\,\mathrm{e}^{-ut}\,\cos\left(f(u)\,\frac{r}{v}\right)$$

$$+ \frac{1}{2\pi r}\,\Theta\left(t - \frac{r}{v}\right)\left\{\int_0^{u_1} + \int_{u_3}^{u_2}\right\}\frac{\mathrm{d}u}{2\pi}\,\mathrm{e}^{-ut}\,\sin\left(f(u)\,\frac{r}{v}\right). \quad (3.20)$$

Although the integrands in Eq.(3.20) are singular, these singularities are only of one-over-square-root type, and are thus integrable.

As we can see from Eqs. (3.3) and (3.5), we also need the spatial derivative of the function $g(t,r)$. It is given by

$$\partial_r\, g(t,r) = -\frac{1}{2\pi v r}\,\delta'\left(t - \frac{r}{v}\right)\left\{\int_0^{u_1} + \int_{u_3}^{u_2}\right\}\frac{\mathrm{d}u}{2\pi}\,\frac{1}{f(u)}\,\mathrm{e}^{-ut}\,\cos\left(f(u)\,\frac{r}{v}\right)$$

$$
\begin{aligned}
&- \frac{1}{2\pi r^2}\,\delta\left(t-\frac{r}{v}\right)\left\{\int_0^{u_1}+\int_{u_3}^{u_2}\right\}\frac{\mathrm{d}u}{2\pi}\,\frac{1}{f(u)}\,\mathrm{e}^{-ut}\,\cos\left(f(u)\,\frac{r}{v}\right)\\
&- \frac{1}{\pi v r}\,\delta\left(t-\frac{r}{v}\right)\left\{\int_0^{u_1}+\int_{u_3}^{u_2}\right\}\frac{\mathrm{d}u}{2\pi}\,\mathrm{e}^{-ut}\,\sin\left(f(u)\,\frac{r}{v}\right)\\
&- \frac{1}{2\pi r^2}\,\Theta\left(t-\frac{r}{v}\right)\left\{\int_0^{u_1}+\int_{u_3}^{u_2}\right\}\frac{\mathrm{d}u}{2\pi}\,\mathrm{e}^{-ut}\,\sin\left(f(u)\,\frac{r}{v}\right)\\
&+ \frac{1}{2\pi v r}\,\Theta\left(t-\frac{r}{v}\right)\left\{\int_0^{u_1}+\int_{u_3}^{u_2}\right\}\frac{\mathrm{d}u}{2\pi}\,f(u)\,\mathrm{e}^{-ut}\,\cos\left(f(u)\,\frac{r}{v}\right)\ , \qquad (3.21)
\end{aligned}
$$

where the integrals are again convergent.

We consider next the Green function $g_1(t,r)$ of Eq.(3.1b) and write it in the form

$$
g_1(t,r)=\int\frac{\mathrm{d}\omega}{2\pi}\,\mathrm{e}^{-\mathrm{i}\omega t}\,\frac{1}{\widetilde{\epsilon}(\omega)}\,\widetilde{g}(\omega,r)\;=\;\mathrm{i}\,\partial_t\,\frac{1}{4\pi r}\int\frac{\mathrm{d}\omega}{2\pi}\,\frac{1}{\omega\,\widetilde{\epsilon}(\omega)}\,\mathrm{e}^{-\mathrm{i}\omega t}\,\mathrm{e}^{\mathrm{i}\,k(\omega)\,r}\ , \qquad (3.22)
$$

where the last integral is convergent for $\omega\to\infty$. More explicitly,

$$
g_1(t,r)=\mathrm{i}\,\partial_t\,\frac{1}{4\pi\epsilon_\infty r}\int\frac{\mathrm{d}\omega}{2\pi}\,\frac{\omega-\omega_3}{(\omega-\omega_1)\,(\omega-\omega_2)}\,\mathrm{e}^{-\mathrm{i}\omega t}\,\mathrm{e}^{\mathrm{i}\,k(\omega)\,r}\ . \qquad (3.23)
$$

In this integral we can deform the integration contour as before and obtain

$$
\begin{aligned}
g_1(t,r)&=\mathrm{i}\,\partial_t\,\frac{\Theta(t-r/v)}{4\pi\epsilon_\infty r}\left\{\int_0^{u_1}\frac{\mathrm{d}u}{2\pi}\,\frac{1}{p(u)}\,\mathrm{e}^{-ut}\,\mathrm{e}^{\mathrm{i}\,f(u)\,r/v}+\int_{u_3}^{u_2}\frac{\mathrm{d}u}{2\pi}\,\frac{1}{p(u)}\,\mathrm{e}^{-ut}\,\mathrm{e}^{\mathrm{i}\,f(u)\,r/v}\right.\\
&\qquad\left.-\int_0^{u_1}\frac{\mathrm{d}u}{2\pi}\,\frac{1}{p(u)}\,\mathrm{e}^{-ut}\,\mathrm{e}^{-\mathrm{i}\,f(u)\,r/v}-\int_{u_3}^{u_2}\frac{\mathrm{d}u}{2\pi}\,\frac{1}{p(u)}\,\mathrm{e}^{-ut}\,\mathrm{e}^{-\mathrm{i}\,f(u)\,r/v}\right\}\\
&=-\,\partial_t\,\frac{\Theta(t-r/v)}{2\pi\epsilon_\infty r}\left\{\int_0^{u_1}+\int_{u_3}^{u_2}\right\}\frac{\mathrm{d}u}{2\pi}\,\frac{1}{p(u)}\,\mathrm{e}^{-ut}\,\sin\left(f(u)\,\frac{r}{v}\right)\ , \qquad (3.24)
\end{aligned}
$$

where

$$
p(u)=-\frac{1}{u}\,f^2(u)=\frac{(u-u_1)\,(u-u_2)}{u-u_3}\ . \qquad (3.25)
$$

The integrand of Eq.(3.24) is singular at $u = u_1$ and $u = u_2$, but, because of the behavior of $f(u)$, the singularities are integrable.

Finally, we consider the Green function $g_2(t, r)$ of Eq. (3.1c):

$$g_2(t,r) = \int \frac{\mathrm{d}\omega}{2\pi}\, \mathrm{e}^{-\mathrm{i}\omega t}\, \widetilde{\epsilon}(\omega)\, \widetilde{g}(\omega, \mathbf{r})\,. \tag{3.26}$$

Since $\widetilde{\epsilon}(\omega) \to \epsilon_\infty = \text{const}$ for $\omega \to \infty$, it is necessary to subtract the constant term, which yields a delta-type contribution to the Green function. We have thus

$$\begin{aligned} g_2(t,r) &= \epsilon_\infty\, g(t,r) + \frac{1}{4\pi r} \int \frac{\mathrm{d}\omega}{2\pi} \left[\widetilde{\epsilon}(\omega) - \epsilon_\infty\right] \mathrm{e}^{-\mathrm{i}\omega t}\, \mathrm{e}^{\mathrm{i}\, k(\omega)\, r}\ , \\ &= \epsilon_\infty\, g(t,r) + \frac{\epsilon_\infty}{4\pi r} \int \frac{\mathrm{d}\omega}{2\pi} \left[\frac{(\omega-\omega_1)\,(\omega-\omega_2)}{\omega\,(\omega-\omega_3)} - 1\right] \mathrm{e}^{-\mathrm{i}\omega t}\, \mathrm{e}^{\mathrm{i} f(\mathrm{i}\omega)\, r/v}\ , \end{aligned} \tag{3.27}$$

where Eq.(3.8) was used to express $\epsilon(\omega)$ and the function $f(\mathrm{i}\omega)$ is given by Eq.(3.19). Evaluation of the last integral presents a certain difficulty, because, at $\omega = \omega_3$, there is a coincidence of the pole in the integrand with the essential singularity in the exponential, resulting from the one-over-square-root singularity in $f(\mathrm{i}\omega)$. As before, based on the asymptotic behavior of the integrand for $\omega \to \infty$, we can deform in the integration contour in Eq.(3.27) to the contours of Fig. 2. In this case, however, we observe that the contribution from the part of the contour encircling the singularity at ω_3 is nonzero. Therefore we break up the contour C'' into two parts: the part encircling the singularity, $C_3(\eta)$, where $\eta \to 0+$ is the radius of the circle, and the remaining part of the contour, C''_-, (see Fig. 2).

Now, by changing as before the integration variable, $u = \mathrm{i}\omega$, we can write

$$\begin{aligned} g_2(t,r) = \ & \epsilon_\infty\, g(t,r) + \frac{\epsilon_\infty}{2\pi r} \left\{ \int_0^{u_1} + \int_{u_3+\eta}^{u_2} \right\} \frac{\mathrm{d}u}{2\pi} \left[\frac{(u-u_1)\,(u-u_2)}{u\,(u-u_3)} - 1\right] \mathrm{e}^{-ut}\, \sin\left(f(u)\,\frac{r}{v}\right) \\ & - \mathrm{i}\,\frac{\epsilon_\infty}{4\pi r} \int_{C_3(\eta)} \frac{\mathrm{d}u}{2\pi} \left[\frac{(u-u_1)\,(u-u_2)}{u\,(u-u_3)} - 1\right] \mathrm{e}^{-ut}\, \mathrm{e}^{\mathrm{i}\, f(u)\, r/v} \\ = \ & \epsilon_\infty\, g(t,r) + \frac{\epsilon_\infty}{2\pi r} \left\{ \int_0^{u_1} + \int_{u_3+\eta}^{u_2} \right\} \frac{\mathrm{d}u}{2\pi} \left[\frac{p(u)}{u} - 1\right] \mathrm{e}^{-ut}\, \sin\left(f(u)\,\frac{r}{v}\right) \\ & - \mathrm{i}\,\frac{\epsilon_\infty}{4\pi r} \int_{C_3(\eta)} \frac{\mathrm{d}u}{2\pi} \left[\frac{p(u)}{u} - 1\right] \mathrm{e}^{-ut}\, \mathrm{e}^{\mathrm{i}\, f(u)\, r/v}\ . \end{aligned} \tag{3.28}$$

By changing the variable to $z = 1/\sqrt{u - u_3}$, we can show that both integrals, over $C_3(\eta)$ and C''_-, are finite in the limit of $\eta \to 0+$. However, despite the fact that the integrals are well defined, their numerical evaluation requires special care. We discuss details of the analytical evaluation and the numerical implementation of Eq.(3.28) in the Supplement to Appendix A1 of the second yearly report.

More details on this part of the project were reported in the second yearly progress report and published in [6].

(D.) Formulations based on the pulse temporal basis functions and band-limited temporal basis functions

Temporal separation densities constitute an important element of the full Galerkin procedure we use in the evaluation of all of the matrix elements of the components of the integral equation kernel for general dispersive media. We have constructed all pertinent temporal separation densities in the analytical form for pulse basis functions and in terms of one dimensional integrals for band-limited basis functions.

The temporal separation density functions

$$\eta^{m(K)}(t) = \eta^{\mu-\nu(K)}(t_1 - t_2) \tag{3.29}$$

depend only on the ***relative*** time $t = t_1 - t_2$, and on one relative temporal index $m = \mu - \nu$, where μ and ν are the indices of the temporal basis functions.

For the *non-overlapping* pulse temporal basis functions given by

$$T^{\mu}(t) = \frac{1}{\Delta t}\,\Theta\left(\frac{t - t_{\mu-1}}{\Delta t}\right)\,\Theta\left(\frac{t_{\mu} - t}{\Delta t}\right)\,, \tag{3.30}$$

where $t_{\mu} = \mu\,\Delta t$, the expressions for the temporal separation density functions (3.30) are quite simple. We find

$$\eta^{m(1)}(t) = \frac{1}{c^2\,\Delta t}\,\left[T^{m+1}(t) - T^{m}(t)\right] = \frac{1}{c^2(\Delta t)^2}\,s(\xi) = -\frac{1}{(c\,\Delta t)^2}\,s\left(\frac{t - t_m}{\Delta t}\right) \tag{3,31a}$$

$$\eta^{m(2)}(t) = c\int_{t}^{\infty} \mathrm{d}\tau\,\eta^{m(3)}(\tau) = H(\xi) = H\left(\frac{t - t_m}{\Delta t}\right)\,, \tag{3.31b}$$

$$\eta^{m(3)}(t) = \frac{1}{c\,\Delta t}\,h(\xi) = \frac{1}{c\,\Delta t}\,h\left(\frac{t - t_m}{\Delta t}\right)\,, \tag{3.31c}$$

$$\begin{aligned}\eta^{m(4)}(t) &= -\frac{1}{c^2\,(\Delta t)^3}\,\left[2\delta(\xi) - \delta(\xi - 1) - \delta(\xi + 1)\right] \\ &= -\frac{1}{(c\,\Delta t)^2}\,\left[2\,\delta(t - t_m) - \delta(t - t_{m+1}) - \delta(t - t_{m-1})\right]\,,\end{aligned} \tag{3.31d}$$

$$\frac{\partial \eta^{m(1)}(t)}{\partial t} = -\eta^{m(4)}(t) = \frac{1}{\Delta t}\,\frac{\partial \eta^{m(1)}(\xi)}{\partial \xi} \tag{3.31e}$$

$$\frac{\partial}{\partial t}\eta^{m(2)}(t) = -c\eta^{m(3)}(t)\,, \tag{3.31f}$$

$$\frac{\partial \eta^{m(3)}(t)}{\partial t} = c\eta^{m(1)}(t), \tag{3.31g}$$

where

$$\xi = \frac{t}{\Delta t} - m = \frac{t}{\Delta t} - (\mu - \nu)\,, \tag{3.32}$$

$$s(\xi) = 2\Theta(\xi) - \Theta(\xi - 1) - \Theta(\xi + 1)\,, \tag{3.33}$$

$$h(\xi) = (1 - |\xi|)\,\Theta(1 - |\xi|)\,, \tag{3.34}$$

$$H(\xi) = \begin{cases} 0 & \text{for } \xi \geq 1\,, \\ \frac{1}{2}(1-\xi)^2 & \text{for } 0 \leq \xi \leq 1\,, \\ 1 - \frac{1}{2}(1+\xi)^2 & \text{for } -1 \leq \xi \leq 0\,, \\ 1 & \text{for } \xi \leq -1 \end{cases} \tag{3.35}$$

$$\frac{\partial}{\partial \xi} s(\xi) = 2\delta(\xi) - \delta(\xi - 1) - \delta(\xi + 1)\,, \tag{3.36}$$

$$\frac{\partial}{\partial \xi} h(\xi) = -s(\xi)\,, \tag{3.37}$$

$$\frac{\partial}{\partial \xi} H(\xi) = -h(\xi)\,. \tag{3.38}$$

In Fig. 3 we display graphs of the the first three temporal separation density functions.

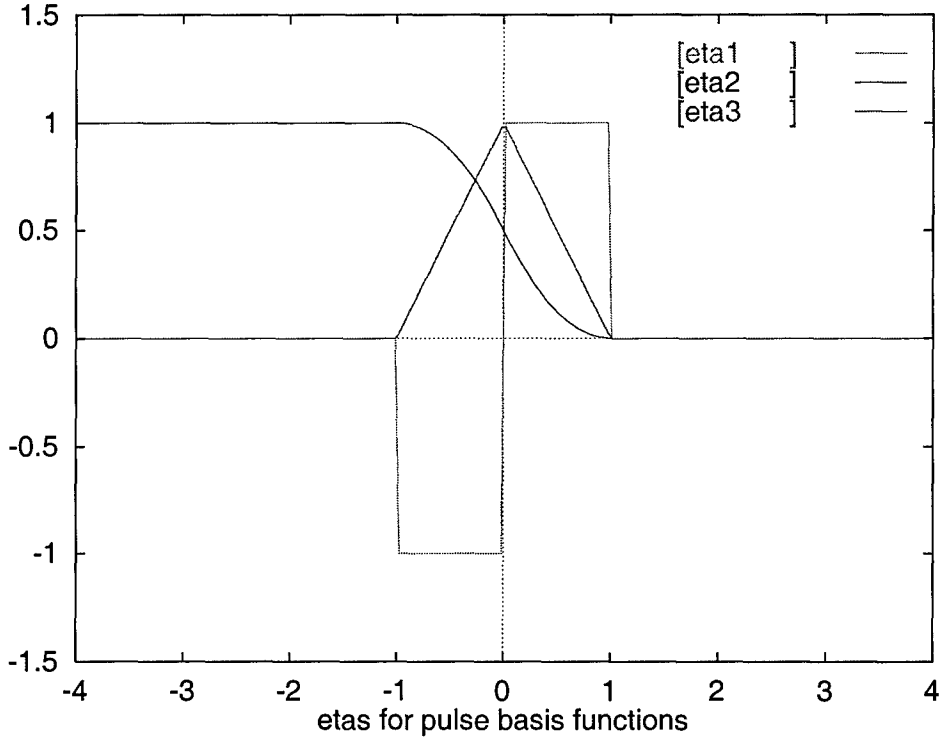

Fig. 3: η_1, η_2, and η_3 functions for the pulse basis functions.

In the following we discuss aspects of the derivation of the temporal separation density functions (3.29), in terms of the band-limited basis functions (APSWFs).

The rationale for using such basis functions is as follows: The block ***lower-triangular*** structure of the impedance matrix in time indices from the causality of the Green function

($G(t, \mathbf{r}) = 0$ for $t < 0$) provided the temporal basis functions $T_\mu(t) \equiv T(t - \mu\,\Delta t)$ do not overlap. Such as restriction of the function T to short time support, however, is in conflict with the assumption of its band-limited property, which is essential in ensuring high-frequency stability of the solution.

In this situation the best possible solution appears to make the temporal basis functions band-limited and approximately of finite (but not necessarily short) time support, and restore the lower-triangularity of the impedance matrix by other means – namely, by temporal extrapolation techniques. The required features can be satisfied to a good accuracy by the approximate prolate spheroidal wave function (APSWF) [2].

We assume that the maximum frequency in the problem is $f_0 = \omega_0/(2\pi)$. The time step is then chosen as

$$\Delta t = \frac{1}{2 s f_0} = \frac{\pi}{s\,\omega_0}\ , \tag{3.39}$$

where $s \simeq 10$ is the oversampling rate. This choice is dictated by the condition that Δt should be of the order of $c\,\Delta r$, where the spatial resolution Δr is of order of $\lambda_0/10$, where λ_0 is the wavelength corresponding to the maximum frequency f_0.

With the parameters f_0 and s, the APSWF $T(t)$ is defined as

$$T(t) = \frac{\sin(\pi\, t/\Delta t)}{\pi\, t/\Delta t}\ \frac{\sin(a\,\sqrt{(t/N\,\Delta t)^2 - 1})}{\sinh(a)\,\sqrt{(t/N\,\Delta t)^2 - 1}}\ , \tag{3.40}$$

where $N \geq 1$ is the *APSWF width*, and

$$a = \pi\, N\, \frac{s-1}{s} \tag{3.41}$$

is called the time-bandwidth product of the APSWF. As shown by Eq.(3.40), the APSWF is the oscillatory sinc function modulated by a smooth factor, rapidly vanishing for $|t| \gtrsim N\,\Delta t$.

Figs. 4a and 4b show the APSWF $T(t)$ for $f_0 = 1\,\mathrm{GHz}$, $s = 10$, and $N = 5$, for which $\Delta t = 0.05\,\mathrm{ns}$, and $a = 14.14$. The APSWF is plotted there as a function of $t/\Delta t$, in the linear and logarithmic scales.

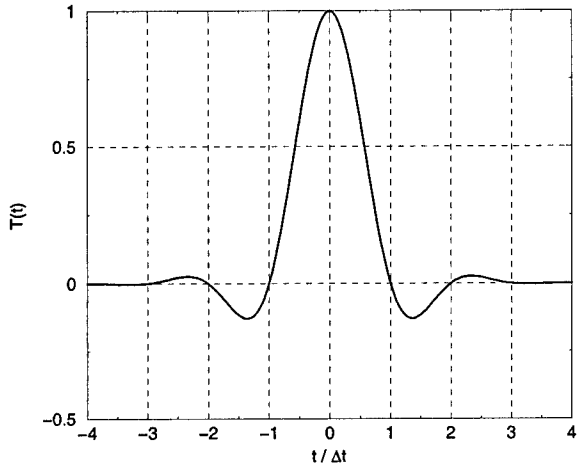

Fig. 4a: The function $T(t)$ plotted with t in units of Δt.

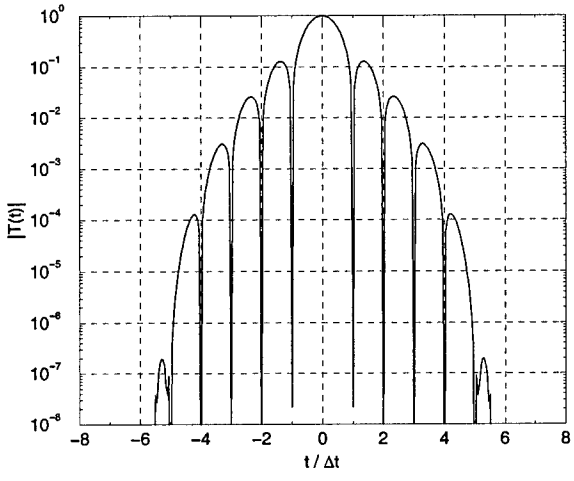

Fig. 4b: The absolution value of the function $T(t)$ plotted in the logarithmic scale.

A difficulty arising when APSWF are used as temporal basis functions is that the basis functions T_μ and T_ν for different time steps $\mu \neq \nu$ overlap. As a consequence, the resulting impedance matrix is not block lower-triangular, i.e., $A^{\mu\nu} \neq 0$ for $\mu < \nu$, or, physically, that the values of the current at a given times step μ depend on current values for future times, $\nu > \mu$. However, the block lower-triangularity may be recovered by extrapolating the current from the past to future values. A good accuracy can be obtained due to the fact that the current is a band-limited function of time. The result of the extrapolation is that the original (not block lower-triangular matrix) can be replaced by a new matrix $\widehat{A}^{\mu\nu}$ which is block lower-triangular. That matrix is computed as

$$\widehat{A}^{\mu\nu} = \begin{cases} A^{\mu\nu} & \text{for } \nu \leq \mu - N_{\mathrm{p}} \ , \\ A^{\mu\nu} + \sum_{\kappa=\mu+1}^{\mu+N_{\mathrm{f}}} A^{\mu\kappa} \, H^{\mu-\kappa,\kappa-\nu} & \text{for } \mu - N_{\mathrm{p}} + 1 \leq \nu \leq \mu \ . \end{cases} \tag{3.42}$$

Here $H^{\mu,\nu}$ is matrix of coefficients obtained by solving a set of least-squares equations which, physically, represent the condition that future values of a set of periodic band-limited functions are represented, with the minimum error, as linear combinations of their past values. In Eq.(3.42) N_{f} is the number of required future values, and N_{p} the number of past values used in the extrapolation. While N_{f} (typically about 5) is determined by the width of the temporal support of $T(t)$ (i.e., by the APSWF width), the number N_{p} of past steps can be adjusted to reduce the extrapolation error to the desired tolerance; a typical value of N_{p} is about 10. Higher values of N_{p} provide a better accuracy, but increase the computational cost of evaluating the modified matrix (3.42). On the other hand, $\widehat{A}^{\mu\nu}$ has to be computed only once, and the resulting computational cost is not significant.

In Figs. 5a to 5d we display the plots of the temporal separation densities computed with the temporal basis functions (3.40).

We note that, since the temporal separation densities $\eta^{\mu(j)}$ have the form

$$\eta^{\mu(j)}(t) = \eta^{0(j)}(t - \mu\Delta t), \qquad j = 1, 2, 3, 4\ ,$$

and the functions $\eta^{0(j)}(t)$ practically vanish outside certain interval $[-T_{\max}, T_{\max}]$, it is sufficient to tabulate them in that interval, and construct other functions by translation.

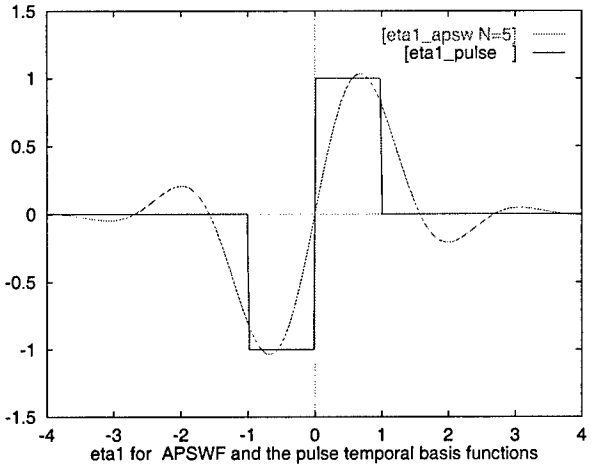

Fig. 5a: The function $\eta^{0(1)}(t)$ plotted with t in units of Δt.

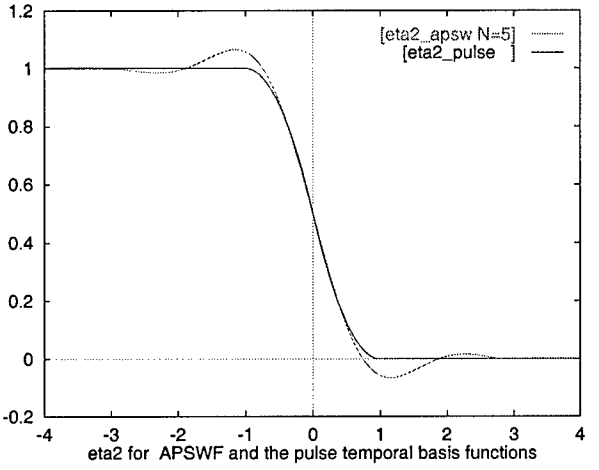

Fig. 5b: The function $\eta^{0(2)}(t)$ plotted with t in units of Δt.

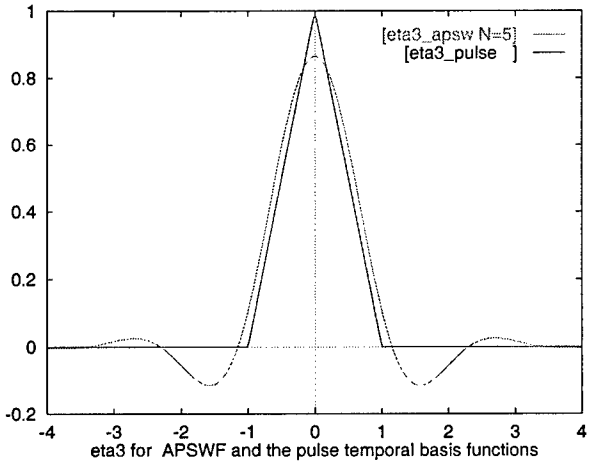

Fig. 5c: The function $\eta^{0(3)}(t)$ plotted with t in units of Δt.

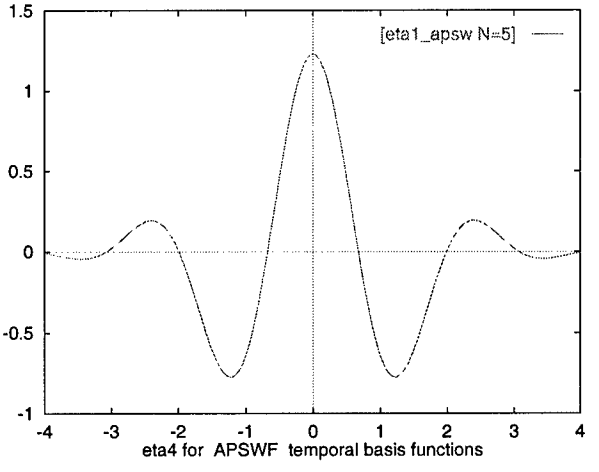

Fig. 5d: The function $\eta^{0(4)}(t)$ plotted with t in units of Δt.

More details on this part of the project were reported in the third yearly progress report and published in [8].

(E.) Regularization of low-frequency solutions of integral equations.

We developed and implemented algorithms necessary for **regularization of low-frequency solutions of integral equations.** Although these methods are originally formulated in frequency domain, we have been motivated by their applicability to time-domain (TD) integral equation methods.

One of the critical problems in the implementation of TD integral equations is their stability for long evolution times. It is known that there are two types of TD integral equations instabilities: those arising from high- and low-frequency phenomena.

The high-frequency instabilities manifest themselves as non-physical rapid oscillations in the solution, of amplitude increasing with time. They can be reduced or eliminated by limiting the bandwidth of the incident signal, and ensuring that no high frequency signals are introduced as the result of time evolution.

The low-frequency instabilities are due the appearance of low- ("zero-") frequency (almost static) solenoidal solutions which do not generate tangential electric fields, and may therefore contaminate the correct solution (at least in the formulation based on electric-field equations, which are based on the boundary conditions for tangential electric field components). Methods of eliminating these parasitic admixtures are based on separating the solution space into two subspaces: (i) that spanned by divergence-free (solenoidal) basis functions and the remainder space, and (ii) the remainder space. An effective procedure is then to simply remove static solution components from the subspace (i) at each evolution step.

Thus, the approaches to eliminating low-frequency instabilities in TD integral equations are based on the same solution space decomposition methods as those used in the low-frequency limit in frequency domain.

Our main focus was on the development of efficient numerical methods of analyzing topology of complex geometries and their surface meshes. These operations are exactly the same in the context of frequency-domain and time-domain approaches, and in both cases lead to construction of of solenoidal and remainder basis functions.

The main outcome of our work was an efficient algorithm for constructing basis functions of the classes (i) and (ii), as mentioned above. It is applicable to triangular surface meshes and basis functions associated with the mesh edges. For geometries characterized by topologies with a limited number of connected components and "handles", the computational cost of the construction is of order $O(E)$, where E is the number of edges in the mesh.

We have implemented the algorithm as a set of geometry processing functions carrying out the required topological analysis (available also as free-standing utilities), and as a set of functions for constructing a "low-frequency preconditioner" applicable to frequency-domain integral equations. The topological analysis routines can be directly applied to the analysis in time domain. Our implementation has been tested on many complex and large size geometries of various topologies, including multiple components and many handles.

We believe that the developed algorithm methods are also of interest in the more general context of computational topology, and its applications in biology and chemistry (topology of macromolecules, etc.), as well as cosmology (structure of galaxies).

As typical results, we show geometries created by our topological analysis routines applied to the surface (of genus 4) displayed in Fig. 6. This geometry is triangulated with about 240,000 edges.

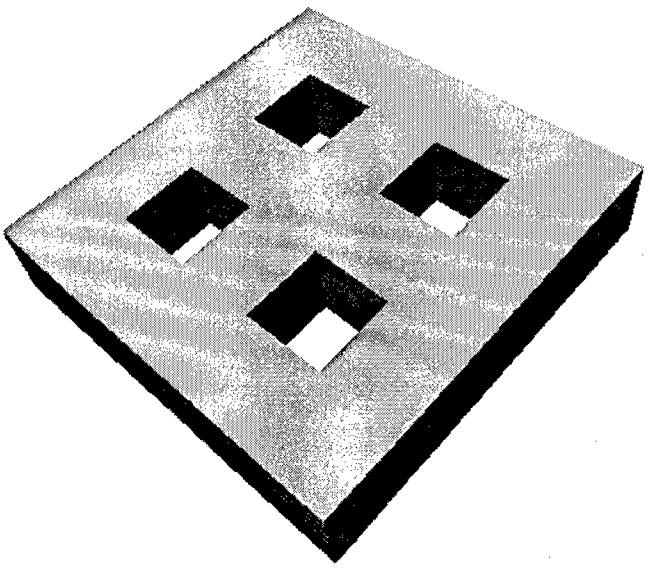

Fig. 6: The geometry used in the topological analysis and construction of basis functions.

Fig. 7 exhibits the geometry created by our utility `genloop`, which constructs topologically nontrivial loop paths. These paths are sequences of segments of the geometry dual to the original geometry; they define a set of "nontrivial" solenoidal basis functions. The other, "trivial", loops are those encircling all interior vertices of the mesh.

Fig. 8 shows the geometry obtained by using the utility `gentree`, which creates tree meshes. These meshes specify basis functions belonging to the "remainder" space of non-solenoidal solutions. In this case, in order to be able to visualize the mesh, we used a much coarser surface discretization, with less than 4000 edges.

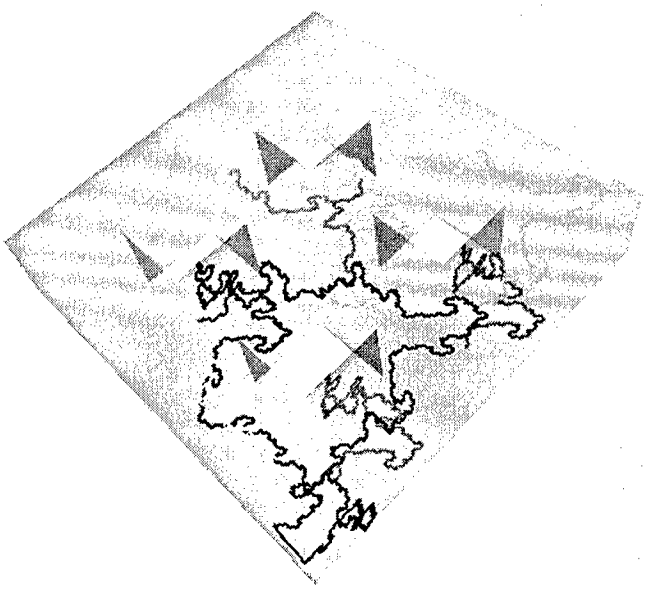

Fig. 7: The geometry showing nontrivial loops (defining solenoidal basis functions) for the geometry of Fig. 6.

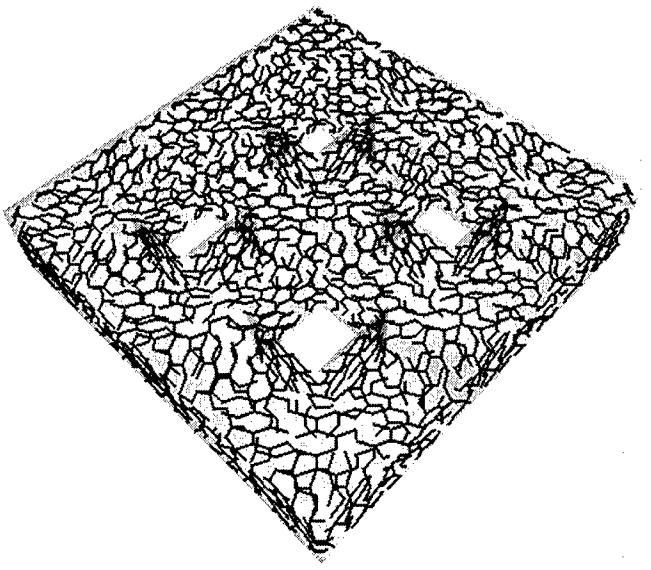

Fig. 8: The geometry showing trees, defining "remainder" basis functions for the geometry of Fig. 6.

(F.) Fast Solution Algorithms Applicable to Finite Periodic and Partially Periodic Systems

We designed and partly implemented a set of fast solution algorithms applicable to finite periodic and partially periodic systems, such as antenna arrays.

The algorithms take advantage of the block-Toeplitz structure of the impedance matrix resulting from the periodicity of the scatterer. They can be applied either to the uncompressed MoM impedance matrix or in conjunction with FMM or FFT-based compression, resulting in what we call Toeplitz-MoM, Toeplitz-FMM, and Toeplitz-FFT solution procedures.

The main effect of the block-Toeplitz structure of the matrix is a dramatic reduction in required memory, due to elimination of redundant matrix blocks and other storage components associated with identical elements of the periodic array. The matrix-vector multiplication complexity of the algorithms does not change significantly (except that it is much reduced in the Toeplitz-MoM approach; that algorithm, however, is in practice applicable only to relatively small small subsystems, with $\lesssim 1000$ unknowns).

We carried out a thorough analysis of the storage requirement and matrix-vector multiplication complexity of the three block-Toeplitz algorithms, both theoretically (on the basis of the structure of the algorithms) and empirically (based on our preliminary algorithm implementation). A typical result is shown in Fig. 9: it is the required storage in Toeplitz-FMM and Toeplitz-FFT algorithms as a function of the number n in a single array element, for several values of the number m of array elements.

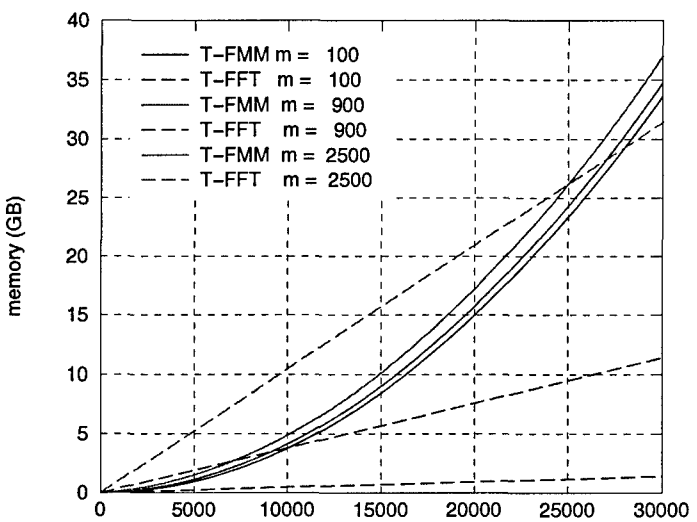

Fig. 9: Required storage in Toeplitz-FMM and Toeplitz-FFT algorithms as a function of n for several values of m (corresponding, e.g., to 10×10, 30×30, and 50×50 arrays).

These plots show that the Toeplitz-FFT grows faster than for Toeplitz-FFT with the increasing m, but slower (linearly, rather than quadratically) as a function of n.

Results of this type and provide valuable information on the regions of applicability of the individual Toeplitz methods. In particular, Fig. 10 shows the ratio of the required storage for the Toeplitz-FMM algorithm to that of the Toeplitz-FFT algorithm.

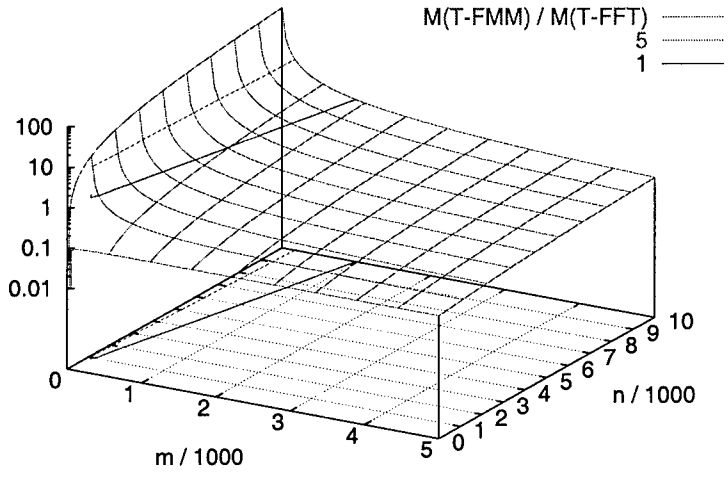

Fig. 10: Ratio of the required storage for Toeplitz-FMM and Toeplitz-FFT algorithms, plotted as a function of m and n (in thousands). Contours for ratios 1 and 5 are also plotted.

We can summarize the main results by stating that:

- The Toeplitz-MoM approach is preferable for a large number of small elements (small number of unknowns per element), where it is much faster than the other methods, and the required storage is still reasonable.
- The Toeplitz-FMM algorithm is preferable for a large number of "medium-size" array elements; a large number of unknowns per element and highly sub-wavelength discretization incur large costs due to the near-field storage.
- The Toeplitz-FFT procedure is preferable for a moderate number of elements with a large number of unknowns per element and possibly sub-wavelength discretization, approximately when the ratio n/m exceeds 10.

More details on this part of the projects were reported in the second yearly progress report and published in [7].

(G.) Generalization to incident waves given as superpositions of Hermite polynomials

We have enhanced our frequency- and time-domain codes simulation capabilities to include numerically efficient modeling of specific time-localized waveforms, such as **linear combinations of Hermite polynomials** or **approximate prolate spheroidal wave functions**.

There is a need for such particular solver numerical capability in the context of several current and future medical and military potential applications, involving, in particular, detection of concealed small arms.

In order to be in a better position to analyze such problems, we derived compact analytical expressions for the projections (on the spatial basis functions) of the incident wave represented as a linear superposition of Hermite polynomials in temporal and spatial variables.

A particular example of practical interest belonging to this class of waveforms is the "Mexican hat" waveform, expressible as a linear superposition of Hermite polynomials up to the second order.

We implemented the resulting formulation in the code module generating the incident wave projection on the Rao-Glisson-Wilton (RWG) basis functions defined on triangular patches, and on pulse or band-limited temporal basis functions. The RGW basis function consists of a pair of "half basis functions" defined over a triangle T and associated with the edge l_m (or, equivalently, with the vertex v_m facing the edge l_m)

$$\mathbf{\Psi}_\alpha(\mathbf{r}) = \frac{1}{h_\alpha}(\mathbf{r} - \mathbf{r}_m)\,\chi(\mathbf{r}) \ , \tag{3.43}$$

where χ is the characteristic function of the triangle.

The incident wave is assumed in the form of a linear superposition of Hermite polynomials H_m

$$\mathbf{E}^{(\mathrm{inc})}(\mathbf{r},t) = \sum_{m=0}^{M} a_m \,\mathrm{H}_m(\gamma\,(\mathbf{k}_0\cdot\mathbf{r} - c\,t)) \tag{3.44}$$

of the argument $\gamma\,(\mathbf{k}_0\cdot\mathbf{r} - c\,t)$, with $|\mathbf{k}_0| = 1$, and with a scale parameter γ.

Evaluation of the incident wave projection required an efficient and numerically stable algorithm for computing convolutions of Hermite polynomials with the basis functions (3.43). We have derived analytic expressions in the form which is easily amenable to numerical implementation. Below we discuss the elements of the derivation for the $m = 0$ term of the series (3.44). Each m-th term can be constructed in terms of the derivative of the $(m-1)$-th term.

The projection $B_{\alpha\mu}$ of the incident wave is given by

$$B_{\alpha\mu} = \int\limits_T \mathrm{d}S \int \mathrm{d}t\, \mathrm{e}^{-\gamma\,(\mathbf{k}_0\cdot\mathbf{r} - c\,t)^2}\, \mathbf{\Psi}_\alpha(\mathbf{r})\, \Phi_\mu(t) \ ,$$

where $\Phi_\mu(t)$ is a temporal basis function, chosen as a rectangular pulse or a band-limited prolate spheroidal wave function.

We have carried out integrations over the barycentric coordinates (ξ_1, ξ_2) (with $0 \leq \xi_1 \leq 1, 0 \leq \xi_2 \leq 1, 0 \leq \xi_1 + \xi_2 \leq 1$) analytically. In these coordinates the projection $B_{\alpha\mu}$ is given by

$$B_{\alpha\mu} = 2\,A \iint\limits_T \mathrm{d}\xi_1\,\mathrm{d}\xi_2 \int \mathrm{d}t\,\mathrm{e}^{-(a\xi_1+b\xi_2+c)^2}\,(\mathbf{a}_1\,\xi_1 + \mathbf{a}_2\,\xi_2)\,\Phi_\mu(t)\ ,$$

where A is the triangle area and a, b, and c are expressible in terms of the parameters of the incident wave and have quadratic dependence on t.

We note that the resulting expressions are difficult to program in the double limit when the parameters a and b tend to zero simultaneously.

We have derived suitable, numerically stable Taylor expansions for these functions by expressing them in terms of auxiliary functions $I_0(a,b,c)$ and $F_0(a,c)$,

$$I_0(a,b,c) = \frac{\sqrt{\pi}}{2} \int\limits_0^1 \mathrm{d}\xi_1 \int\limits_0^{1-\xi_1} \mathrm{d}\xi_2\,\mathrm{erf}(a\xi_1 + b\xi_2 + c)\ ,$$

$$I_1(a,b,c) = \int\limits_0^1 \mathrm{d}\xi_1 \int\limits_0^{1-\xi_1} \mathrm{d}\xi_2\,\xi_1\,\mathrm{e}^{-(a\xi_1+b\xi_2+c)^2} = \frac{\partial}{\partial a}\,I_0(a,b,c)\ ,$$

$$I_2(a,b,c) = \int\limits_0^1 \mathrm{d}\xi_2 \int\limits_0^{1-\xi_1} \mathrm{d}\xi_2\,\xi_2\,\mathrm{e}^{-(a\xi_1+b\xi_2+c)^2} = \frac{\partial}{\partial b}\,I_0(a,b,c) = I_1(b,a,c)\ ,$$

with

$$\frac{\mathrm{d}}{\mathrm{d}x}\,\mathrm{erf}(x) = \frac{2}{\sqrt{\pi}}\,\mathrm{e}^{-x^2}$$

$$I_0(a,b,c) = \frac{F_0(a,c) - F_0(b,c)}{a-b}\ ,$$

$$F_0(a,c) = \frac{H(c+a) - H(c)}{a}\ ,$$

and

$$H(z) = \sqrt{\frac{\pi}{8}}\,\mathrm{erf}(z)\,(2z^2+1) + \frac{z}{4}\,\mathrm{e}^{-z^2}\ .$$

For small arguments we used the following expansions of the functions $H(z)$ and $F_0(a,c)$:

$$H(z) = \frac{1}{2}\,z + \frac{1}{6}\,z^3 - \frac{1}{60}\,z^5 + \frac{1}{420}\,z^7 + \cdots\ ,$$

$$F_0(a,c) = \frac{1}{2}\,\mathrm{e}^{-c^2} + \frac{\sqrt{\pi}}{2}\,c\,\mathrm{erf}(c) + \frac{\sqrt{\pi}}{4}\,\mathrm{erf}(c)\;a + \frac{1}{6}\,\mathrm{e}^{-c^2}\;a^2 - \frac{1}{12}\,c\,\mathrm{e}^{-c^2}\;a^3 + \frac{1}{60}\,c\,\mathrm{e}^{-c^2}\,(2\,c^2-1)\;a^4 + \cdots\ .$$

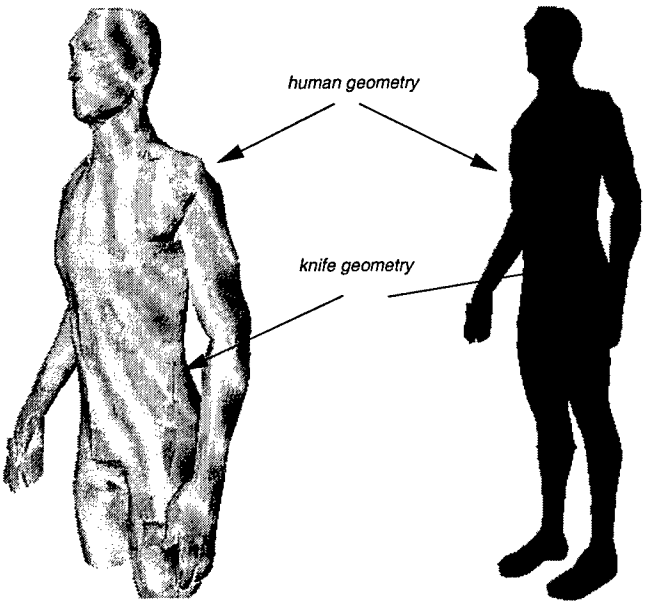

Fig. 11: Representative display of the current distribution on a man with a knife.

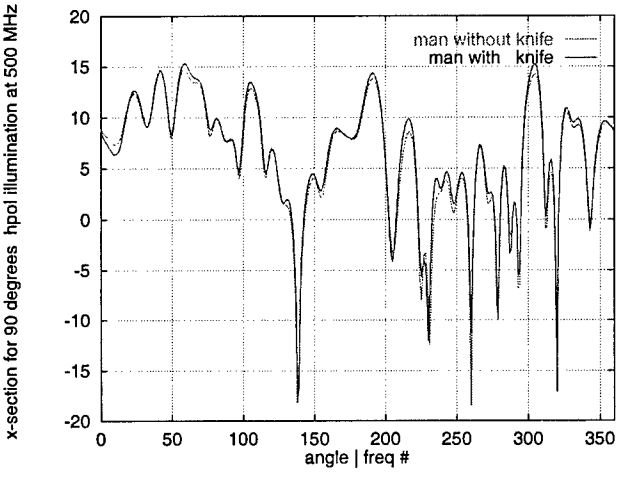

Fig. 12: Comparison of the preliminary results for the radar cross section for a 500 MHz incident wave illuminating a man with and without a knife

We initiated calculations/analysis for representative scenario a man with a concealed knife illuminated with different incident beams given in terms of superposition of Hermite polynomials (Fig. 12 shows a representative display of the electric current induced on such a geometry). This analysis is in progress.

(H.) Work on aspects of foliage penetration problems

We performed several computations to verify the applicability of the developed code to the analysis of SAR returns from scenes containing objects of military interest concealed under foliage.

To perform more realistic simulations than the plane wave (or superposition of plane waves) illumination, we added the antenna modeling option into our integral equation solver. We model the transmitting and receiving elements as delta-gap structures built into a Rao-Wilton-Glisson basis function. The transmitting element at an edge, say, α is characterized by a voltage source V_0 and a (connected in series) resistance R_α. The receiving delta-gap at an edge, say, β, is defined similarly to the transmitting one, but without the voltage source, i.e., it represents only the resistive load R_β. The goal of the MoM antenna modeling is to obtain predictions for the antenna parameters of a single antenna or a system of antennas, interacting with themselves and/or with other objects. Of main interest are parameters associated with the antenna transmitting or receiving ports, such as the input impedance, received voltage, transfer function, etc.

We constructed geometries composed of irregularly shaped ground, trees, and a perfectly conducting object located under the trees. We also modeled the transmitting and receiving horn antennas.

Below we present some of the relevant simulations.

Fig. 13 shows a scene composed of a ground, four trees and a perfectly conducting object of pyramidal shape. The scene is 20 m in size, the trees are approximately 10 m high, the size of the object is 1 m. The computations were performed at 200 MHz. The computational problem size was approximately 450,000 unknowns. The realistic material properties of wood, leaves and soil were assigned to all the objects in the scene. Figs. 14 and 15 show the bistatic and the backscattering cross sections computed with and without the hidden object. Fig. 16 shows the influence of leaves. As anticipated, this influence is negligible at the frequency of 200 MHz.

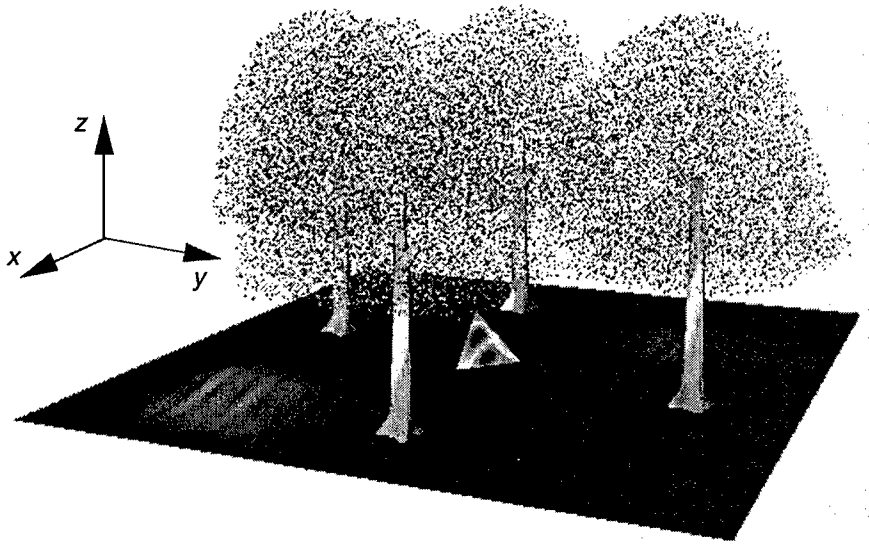

Fig. 13: A scene with a pyramidal object concealed under the foliage.

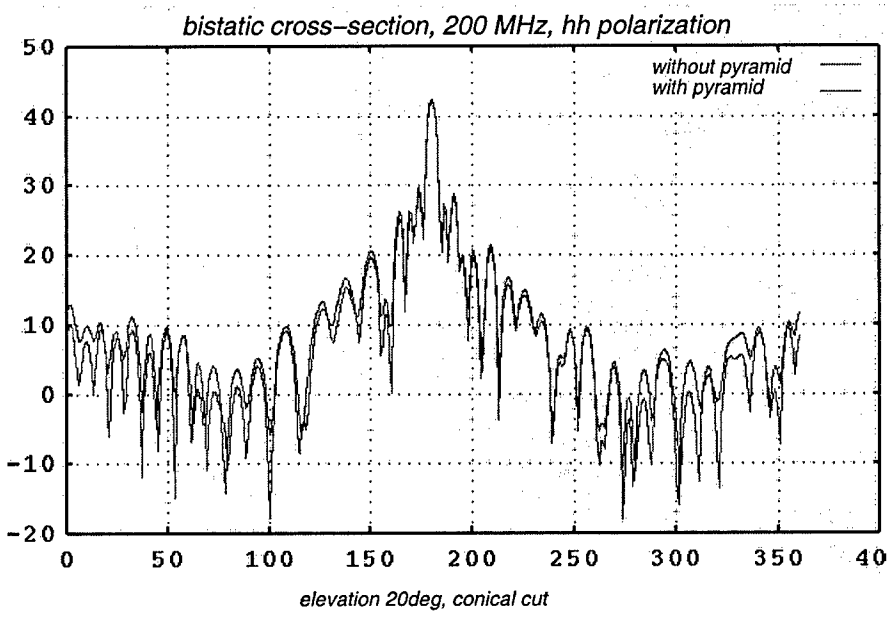

Fig. 14: Bistatic cross section at 200 MHz corresponding to the scene of Fig. 9.

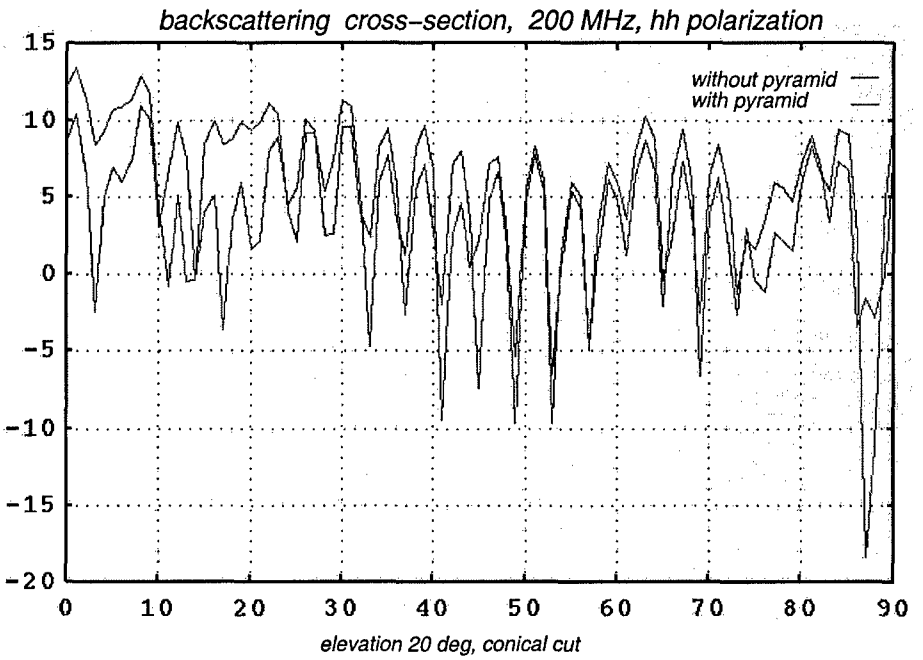

Fig. 15: Backscattering cross section at 200 MHz corresponding to the scene of Fig. 9.

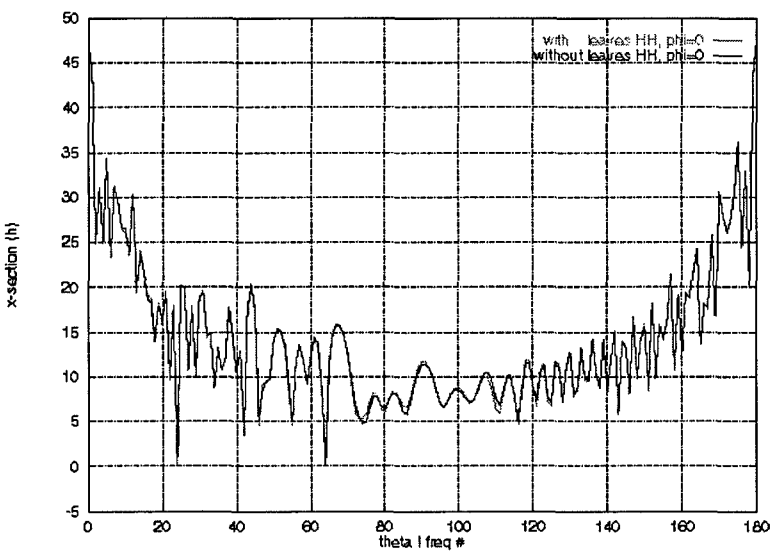

Fig. 16: Effect of leaves in the bistatic cross section at 200 MHz for the scene of Fig.13 .

Subsequently, we constructed a scene composed of uneven ground, twelve trees and a perfectly conducting object of pyramidal shape. The scene was 30 m in size. Two horn antennas, a transmitter and a receiver were placed, one on top of each other, on a 12 m track in front of the scene. The computational size of the problem, at 200 MHz, was approximately 1,000,000 unknowns. The scene is shown in Figs. 17 and 18. Fig. 19 shows the backscattering cross section with and without the concealed object. Figs. 20 and 21 show the voltage drop at the receiver and the transfer function for the system of the transmitter/receiver antennas computed at six positions along the 12 m long track again, in the presence and in the absence of the concealed object.

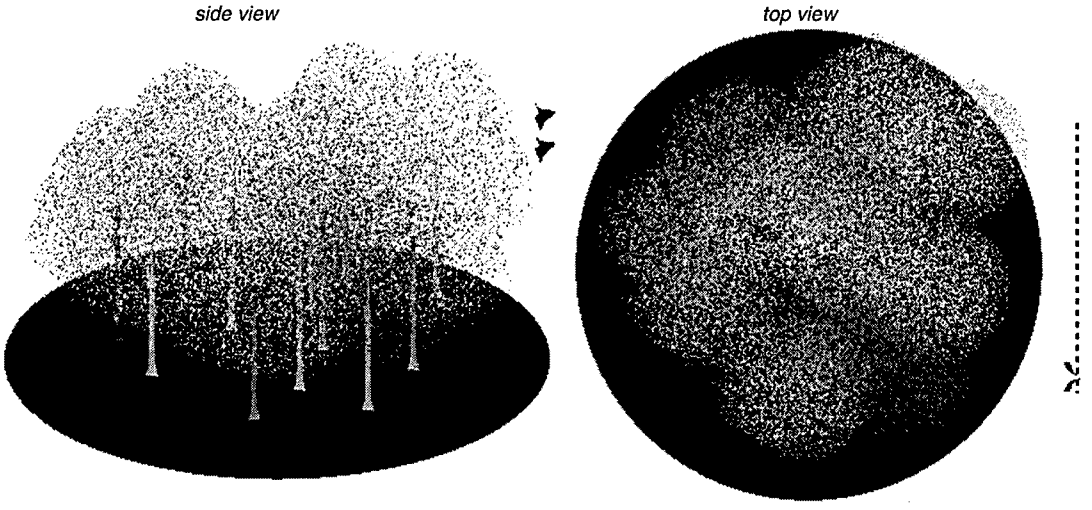

Fig. 17: A scene with a pyramidal object concealed under the foliage and two antennas (a receiver and a transmitter) mounted on a track.

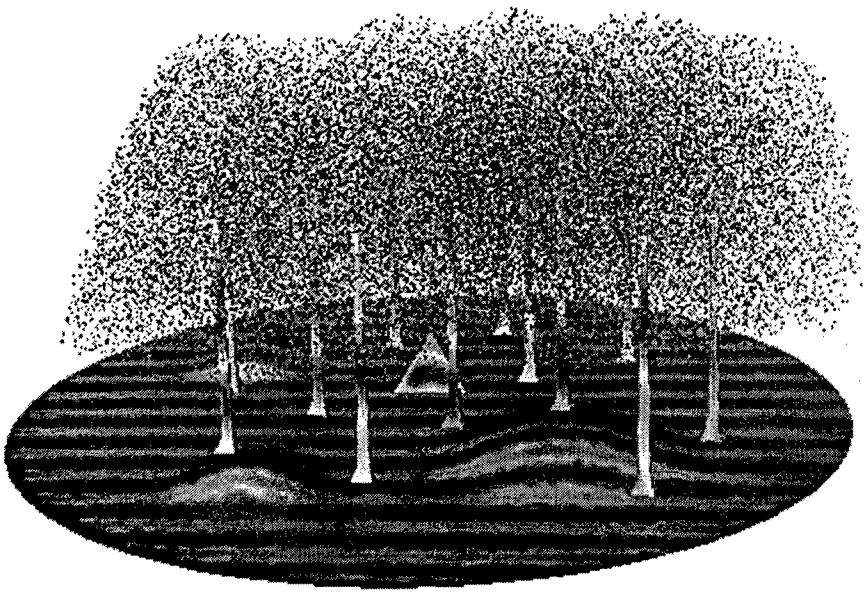

Fig. 18: The same scene as in Fig. 13 with a typical surface current distribution.

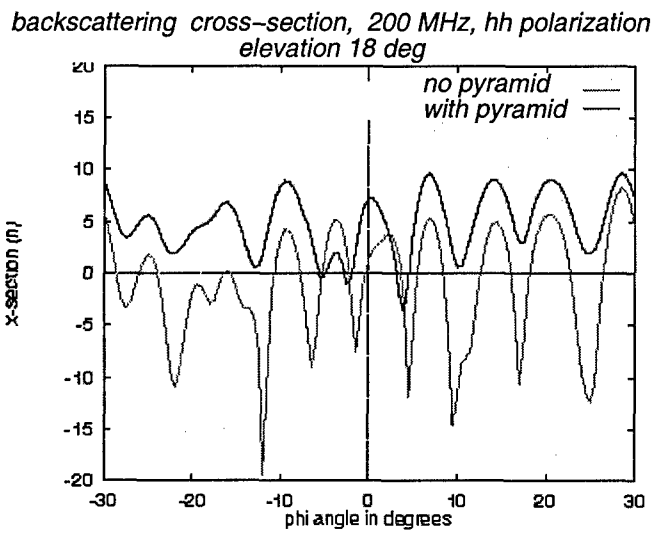

Fig. 19: Backscattering cross section at 200 MHz corresponding to the scene of Fig. 13.

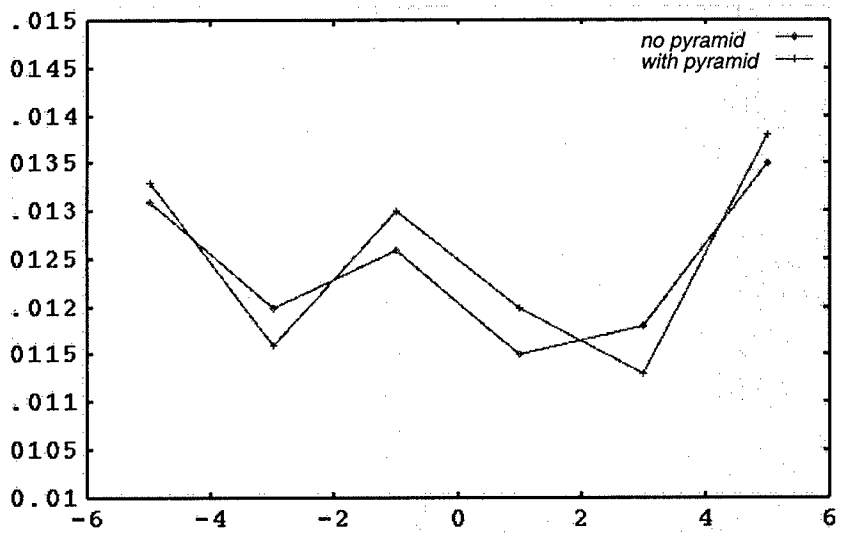

Fig. 20: Voltage drop at the receiver computed at 6 locations along the 12 m long track.

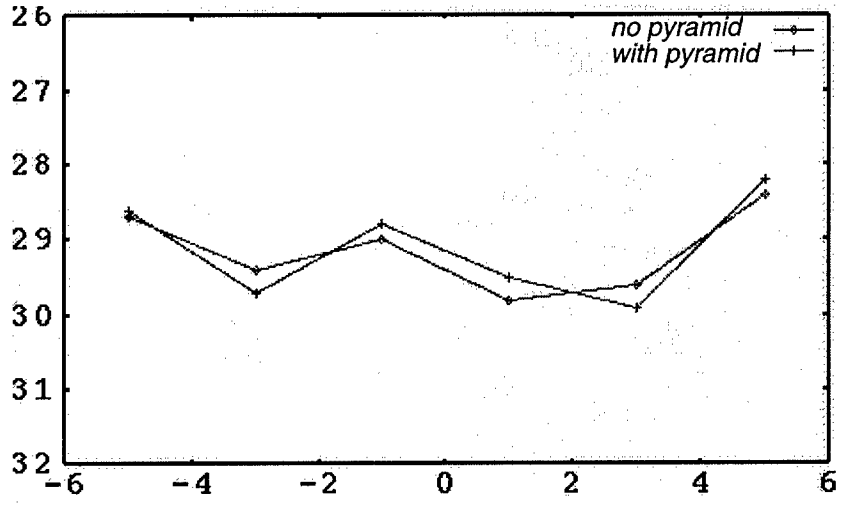

Fig. 21: Transfer function computed at 6 locations along the 12 m long track.

The performed computations indicate the code capability to compute ***routinely*** scattering from large, of the order of one million unknowns, scenes composed of objects of complex shapes and realistic materials.

At present, the code is being used on an Air Force contract to compute SAR returns and to identify material properties of the scene components. The scenes are approximately 30 m in size. The computations are being performed at the frequency range from 100 MHz

to 1 GHz and for multiple (approximately 100) angles of incidence. The computational problem size is approximately 1.5 M unknowns at the frequency of 1 GHz. A novel phase interpolation algorithm (developed on the above mentioned contract and implemented into the code) allows us to perform computations every 10 MHz and to accurately interpolate to 1 MHz intervals. The phase interpolation algorithm allows us to synthesize results not only for relatively narrow-band pulses traditionally used in SAR applications, but also for wide-band pulses.

References

1. E. Bleszynski, M. Bleszynski, and T. Jaroszewicz, "Surface Integral Equations for Electromagnetic Scattering from Impenetrable and Penetrable Sheets", *IEEE Antennas and Propagation Magazine*, Vol. 35, pp. 14-25, 1993.
2. J.J. Knab, "Interpolation of Band-Limited Functions Using the Approximate Prolate Series", *IEEE Trans. Inform. Theory*, Vol. IT-52, pp. 717-720, 1979.
3. A. Yilmaz, K. Aygun, J.M. Jin, and E. Michielssen, "Matching Criteria and the Accuracy of Time Domain Adaptive Method", *in proceedings of the 2002 San Antonio AP IEEE Conference,* Vol. 2, pp. 166-169, July 2002).
4. Dr. Feng Ling and Prof. Vladimir Ochmatovski, *private communication.*
5. E. Bleszynski, M. Bleszynski, and T. Jaroszewicz, "Fast Time-Domain Integral Equations Approach for Wide Band Pulse Propagation in Dispersive Media", *in Ultra-Wideband Short-Pulse Electromagnetics*, Kluver Academic/Plenum Publishers, 2003.
6. E. Bleszynski, M. Bleszynski, and T. Jaroszewicz, "Fast Time-Domain Integral Equation Solver for Dispersive Media", *in Ultra-Wideband Short-Pulse Electromagnetics*, Kluver Academic/Plenum Publishers, 2006, in press.
7. E. Bleszynski, M. Bleszynski, and T. Jaroszewicz, "Block Toeplitz Fast Integral Equation Solver for Large Finite Periodic and Partially Periodic Array Systems", *IECE Trans Electronics*, Vol. E87, No 9, pp. 1586-1594, 2004.
8. E. Bleszynski, M. Bleszynski, and T. Jaroszewicz, "Fast Time Domain Integral Equation Solver for Dispersive Media with Auxiliary Green Functions", in proceedings of the *ACES (Applied Computational Electromagnetics Society) Conference*, Honolulu, HW, 2005.
9. E. Bleszynski, M. Bleszynski, and T. Jaroszewicz, "Application of Fast Time- And Frequency-Domain Integral Equation Methods To Simulation Of Pulse Propagation Through Foliage" in proceedings of the *KIMAS 2003 (IEEE Conference on Knowledge Intensive Multiagent Systems)*, Cambridge, MA, October 2003.
10. E. Bleszynski, M. Bleszynski, and T. Jaroszewicz, "Simulation of Synthetic Aperture (SAR) Returns from Complex Scenes", in proceedings of the *2005 KIMAS (IEEE Conference on Knowledge Intensive Multiagent Systems)*, Cambridge, MA, May 2005.

4. Personnel supported

Dr. Elizabeth Bleszynski is the principal investigator on this effort. Two senior researchers, Dr. Marek Bleszynski and Dr. Thomas Jaroszewicz participate in the effort.

5. Publications

1. E. Bleszynski, M. Bleszynski, and T. Jaroszewicz, "Fast Time-Domain Integral Equations Approach for Wide Band Pulse Propagation in Dispersive Media", *in Ultra-Wideband Short-Pulse Electromagnetics*, Kluver Academic/Plenum Publishers, 2003.
2. E. Bleszynski, M. Bleszynski, and T. Jaroszewicz, "Fast Time-Domain Integral Equation Solver for Dispersive Media", *in Ultra-Wideband Short-Pulse Electromagnetics*, Kluver Academic/Plenum Publishers, 2006, in press.
3. E. Bleszynski, M. Bleszynski, and T. Jaroszewicz, "Block Toeplitz Fast Integral Equation Solver for Large Finite Periodic and Partially Periodic Array Systems", *IECE Trans Electronics*, Vol. E87, No 9, pp. 1586-1594, 2004.
4. E. Bleszynski, M. Bleszynski, and T. Jaroszewicz, "Fast Time Domain Integral Equation Solver for Dispersive Media with Auxiliary Green Functions", in proceedings of the *ACES (Applied Computational Electromagnetics Society) Conference*, Honolulu, HW, 2005.
5. E. Bleszynski, M. Bleszynski, and T. Jaroszewicz, "Application of Fast Time- And Frequency-Domain Integral Equation Methods To Simulation Of Pulse Propagation Through Foliage" in proceedings of the *KIMAS 2003 (IEEE Conference on Knowledge Intensive Multiagent Systems)*, Cambridge, MA, October 2003.
6. E. Bleszynski, M. Bleszynski, and T. Jaroszewicz, "Simulation of Synthetic Aperture (SAR) Returns from Complex Scenes", in proceedings of the *2005 KIMAS (IEEE Conference on Knowledge Intensive Multiagent Systems)*, Cambridge, MA, May 2005.

6. Interactions/Transitions

Presentations at meetings and conferences:

The following ***invited*** presentation were made during the grant period:

1. "Application of Fast Time- And Frequency-Domain Integral Equation Methods to Simulation of Pulse Propagation Through Foliage" IEEE Conference on Knowledge Intensive Multiagent Systems, Cambridge, MA, October 4, 2003,
2. "Fast Time-Domain Integral Equations Approach for Wide Band Pulse Propagation in Dispersive Media", AMEREM Conference, Annapolis, MD , June 2003,
3. "Block-Toeplitz Fast Integral Equation Solver for Large Periodic And Non-Periodic Finite Antenna Array Systems", IEEE Topical Conference on Wireless Applications, Honolulu, HW, October 17, 2003,
4. "Application of Wavefront-Based Method in High Frequency and Time Domain Scattering and Propagation Problems", IEEE Conference on Antennas and Propagation, Dayton, OH, 2003,

5. "Simulation of Synthetic Aperture (SAR) Returns from Complex Scenes", IEEE Conference on Knowledge Intensive Multiagent Systems, Cambridge, MA, May 2005,
6. "Fast Time-Domain Integral Equation Solver for Dispersive Media", EUROEM Conference, Magdeburg Germany July 2005.
7. "Fast Time Domain Integral Equation Solver for Dispersive Media with Auxiliary Green Functions", ACES (Applied Computational Electromagnetics Society) Conference, Honolulu, HW, April 2005,

Consultative and advisory functions:

1. Assistance to Air Force Research Labs, Brooks Air Force base in modeling and analysis of problems in the area of EM interaction with human tissue and foliage penetration (R. Albanese, S. Sherwood, and T. Campbell).
2. Assistance to Titan Corporation; development of the formulation and the code module applicable to the performance analysis and optimization of wide band antennas with dispersive elements (J. Riordan and H. Sze).
3. Assistance to University of Florida in numerical simulations of observables in the context of problems involving detection of tanks under trees (S. Shabanov and T. Olson).
4. An early version of our block Toeplitz time domain integral equation solver has been independently verified and adopted as the Time Domain Adaptive Integral Equation Method by the University of Illinois researches who constructed a code based on this formulation (A. Yilmaz, K. Aygun, J.M. Jin, and E. Michielssen, "Matching Criteria and the Accuracy of Time Domain Adaptive Method", in proceedings of the 2002 San Antonio AP IEEE Conference, Vol. 2, pp. 166-169, July 2002).

Transitions:

The developed formulation and the corresponding solver provide a unique opportunity for the simulation of such problems of interest to the Air Force and DOD as SAR scenes or identification of objects concealed under foliage or, e.g., on a human body. The developed technolody already resulted and was/is being used on two Air Force contracts awarded to Monopole Research.

7. New discoveries

1. Formulation of a novel fast algorithm based on simultaneous compression in space and time, and exhibiting the same competitive performance for dispersive as well as non-dispersive media.

8. Honors/Awards

No honors or awards were received during the grant period.